Am J Physiol Renal Physiol 291: F866–F873, 2006.
First published May 16, 2006; doi:10.1152/ajprenal.00027.2006.

Endothelin and nitric oxide mediate adaptation of the cortical collecting duct to metabolic acidosis

Shuichi Tsuruoka,[1] Seiji Watanabe,[2] Jeffrey M. Purkerson,[2] Akio Fujimura,[1] and George J. Schwartz[2]
[1]*Department of Pharmacology, Jichi Medical School, Tochigi, Japan; and* [2]*Department of Pediatrics, University of Rochester School of Medicine, Rochester, New York*

Submitted 25 January 2006; accepted in final form 10 May 2006

Tsuruoka, Shuichi, Seiji Watanabe, Jeffrey M. Purkerson, Akio Fujimura, and George J. Schwartz. Endothelin and nitric oxide mediate adaptation of the cortical collecting duct to metabolic acidosis. *Am J Physiol Renal Physiol* 291: F866–F873, 2006. First published May 16, 2006; doi:10.1152/ajprenal.00027.2006.—Endothelin (ET) and nitric oxide (NO) modulate ion transport in the kidney. In this study, we defined the function of ET receptor subtypes and the NO guanylate cyclase signaling pathway in mediating the adaptation of the rabbit cortical collecting duct (CCD) to metabolic acidosis. CCDs were perfused in vitro and incubated for 3 h at pH 6.8, and bicarbonate transport or cell pH was measured before and after acid incubation. Luminal chloride was reversibly removed to isolate H^+ and HCO_3^- secretory fluxes and to raise the pH of β-intercalated cells. Acid incubation caused reversal of polarity of net HCO_3^- transport from secretion to absorption, comprised of a 40% increase in H^+ secretion and a 75% decrease in HCO_3^- secretion. The ET_B receptor antagonist BQ-788, as well as the NO synthase inhibitor, N^G-nitro-L-arginine methyl ester (L-NAME), attenuated the adaptive decrease in HCO_3^- secretion by 40%, but only BQ-788 inhibited the adaptive increase in H^+ secretion. There was no effect of inactive D-NAME or the ET_A receptor antagonist BQ-123. Both BQ-788 and L-NAME inhibited the acid-induced inactivation (endocytosis) of the apical Cl^-/HCO_3^- exchanger. The guanylate cyclase inhibitor LY-83583 and cGMP-dependent protein kinase inhibitor KT-5823 affected HCO_3^- transport similarly to L-NAME. These data indicate that signaling via the ET_B receptor regulates the adaptation of the CCD to metabolic acidosis and that the NO guanylate cyclase component of ET_B receptor signaling mediates downregulation of Cl^-/HCO_3^- exchange and HCO_3^- secretion.

tubule microperfusion; endothelin receptor antagonist; nitric oxide synthase inhibitor; cyclic GMP; cyclic GMP-dependent protein kinase

ENDOTHELINS (ET) were first described as vasoactive peptides that regulate regional vascular tone by signaling cells in the cardiovascular system via members of the G protein-coupled receptor family (15a, 45). Since the early 1990s, it has become apparent that ET also regulates sodium-water balance and pH homeostasis in the kidney by directly signaling renal epithelial cells. ET promotes water diuresis by acting to inhibit the hydroosmotic action of vasopressin (22). Several studies implicate ET in the regulation of acid-base homeostasis in the proximal tubule (41) as well as the distal nephron (42, 43). ET modulates NHE3 activity in the proximal tubule and thereby regulation of proton secretion by this segment (13). In the distal nephron, ET-1 is abundantly expressed by collecting ducts (12), as are ET_B receptors (29). ET stimulates distal tubular acidification in the rat (42, 43), and the expression of ET in the kidney is stimulated by metabolic acidosis (44). Mice having a genetically disrupted ET_B receptor experience a more severe acidosis than normal mice in response to acid loading (13). However, a detailed assessment of the regulation of proton vs. bicarbonate transport in the cortical collecting duct (CCD) is lacking.

In many cases, the effects of ET on ion transport processes in nephron segments are mediated by the generation of nitric oxide (NO) resulting from activation of a NO synthase (NOS) (9, 10, 17). In vivo studies suggest that NO induces a natriuresis and diuresis, which is mediated by activation of guanylate cyclase. In the proximal tubule, Wang et al. (41) reported that tubules from neuronal NOS knockout mice exhibited lower fluid and HCO_3^- absorption rates compared with tubules from wild-type mice. Thus NO produced by neuronal NOS in the proximal tubule is likely to stimulate fluid and HCO_3^- absorption. In the CCD NO inhibits Na^+ absorption and vasopressin-stimulated osmotic water permeability (5, 17). The effect of NO on osmotic water permeability is blocked by guanylate cyclase and cGMP-dependent protein kinase (PKG) inhibitors, indicating that the effect of NO is mediated by activation of soluble guanylate cyclase and subsequent activation of PKG by cGMP (6, 17). This cascade results in inhibition of vasopressin-stimulated osmotic water permeability (6, 17).

In the thick ascending limb, endogenous NO inhibits chloride transport (20), and a comparable inhibition is observed using exogenous ET-1 (19). The ET effect is blocked by inhibiting NOS with N^G-nitro-L-arginine methyl ester (L-NAME) (19), suggesting that the effects of ET-1 are mediated by NOS in the thick ascending limb of Henle's loop (9).

NO also regulates pH homeostasis in the distal nephron. In freshly isolated CCDs, NO donors decrease bafilomycin-sensitive H^+-ATPase activity (31). Such inhibition is likely mediated by cGMP because cGMP analogs also inhibit H^+-ATPase activity (31). However, this finding would lead to an expectation of decreased H^+ secretion in the CCD, which could be life threatening in a setting of metabolic acidosis. In contrast, mice deficient in neuronal (n)NOS develop metabolic acidosis (41). In rats inhibition of NO by administration of L-NAME impairs urinary acid excretion after acute NH_4Cl loading (35). CCDs taken from such treated rats showed that net bicarbonate absorption was reduced by 40%. These studies strongly suggest that NO is involved in the maintenance of acid-base homeostasis in the distal nephron; however, it has not been established whether NO regulates proton and/or bicarbonate flux by intercalated cells.

Address for reprint requests and other correspondence: G. J. Schwartz, Pediatric Nephrology, Box 777, Univ. of Rochester Medical Center, 601 Elmwood Ave., Rochester, NY 14642 (e-mail: George_Schwartz@urmc.rochester.edu).

The costs of publication of this article were defrayed in part by the payment of page charges. The article must therefore be hereby marked "*advertisement*" in accordance with 18 U.S.C. Section 1734 solely to indicate this fact.

In this study, we examine whether the changes in H^+/HCO_3^- secretion fluxes induced by acidosis are regulated by ET receptor signaling via the NO-guanylate cyclase pathway. We made use of in vitro acid incubation of CCDs that recapitulates the findings of 3 days of in vivo acid loading (21). CCDs taken from normal rabbits secrete net HCO_3^-, and this net flux is made up of a small H^+ secretory flux that is outstripped by a much larger HCO_3^- secretory flux (26, 33). The adaptation to acidosis is associated with both a modest increase in H^+ secretory flux and a large decrease in HCO_3^- secretory flux, with the resultant sum of fluxes being the secretion of net protons (26, 33); that is, a reversal in polarity of net HCO_3^- transport.

METHODS

Animals. Female New Zealand white rabbits ($n = 49$) weighing 1.6–2.5 (mean 2.04) kg were maintained on standard laboratory chow (Japan Clea) with free access to water (33). Animals were killed by intracardiac injection of 130 mg pentobarbital sodium after premedication with ketamine (44 mg/kg) and xylazine (5 mg/kg). Urine was obtained postmortem by bladder tap; urine pH averaged 7.96 ± 0.02 (SE, $n = 49$).

Microperfusion of CCDs. CCDs were microdissected and microperfused as performed in this laboratory (26, 33). The average tubule length was 0.9 ± 0.1 mm. Equilibration and transport were performed using Burg's solution in the perfusate and bath, containing (in mM) 120 NaCl, 25 $NaHCO_3$, 2.5 K_2HPO_4, 2 $CaCl_2$, 1.2 $MgSO_4$, 5.5 D-glucose, 1 trisodium citrate, 4 sodium lactate, and 6 L-alanine, 290 ± 2 mosmol/kgH_2O, and gassed with 94% O_2-6% CO_2, yielding a pH of 7.4 at 37°C (26, 33, 34). Bath was continually exchanged at 14 ml/h by a peristaltic pump. Luminal perfusion rate was maintained at 1.5–2.1 nl/min.

Incubation for 3 h at low pH (pH 6.8 in both luminal and bathing solutions) has been previously described (21). Briefly, the luminal solution contained DMEM without $NaHCO_3$ (GIBCO, BRL, Gaithersburg, MD), Burg's solution, and dissection solution (Burg's solution with 25 mM $NaHCO_3$ replaced by NaCl) in a ratio of 3:2:4, respectively. The bathing solution was similar except that it also contained 30 U/ml penicillin, 30 μg/ml streptomycin, and 3.3% fetal calf serum (GIBCO, BRL) (21, 33, 46). Incubation at pH 6.8 in vitro yields a physiology comparable to 3 days of acidosis in vivo and reverses the polarity of HCO_3^- flux from net secretion to net absorption (21, 26, 33).

Bicarbonate transport. Triplicate collections of 12–15 nl of tubular fluid were made under water saturated mineral oil and analyzed for HCO_3^- using a Nanoflo (WPI, Sarasota, FL) (26, 33, 35, 36). Net HCO_3^- was calculated as $J_{HCO3} = (C_O - C_L) \times (V_L/L)$, where C_O and C_L are the HCO_3^- concentrations of perfused and collected fluid, respectively, V_L is the rate of collected fluid, and L is the length of the tubule (mm) (26, 33). When HCO_3^- transport (J_{HCO3}) is >0, there is net HCO_3^- absorption; when J_{HCO3} is <0, there is net HCO_3^- secretion. To distinguish between unidirectional H^+ and HCO_3^- secretion after net HCO_3^- transport is measured, luminal Cl^- was replaced by gluconate (21). In this maneuver, HCO_3^- is not secreted, thereby uncovering the unidirectional H^+ secretory flux. Subtracting this H^+ secretory flux from the net bicarbonate transport flux reveals the HCO_3^- secretory flux.

Measurements were repeated after the 3-h incubation and compared with preincubation values. In most of the experiments, an agent was introduced in the bath for 30 min at pH 7.4 before being added to the pH 6.8 bathing solution for the 3-h incubation (21, 26). The agents included BQ-788 (1 μM, Sigma, ET_B receptor antagonist) (8), BQ-123 (1–10 μM, Sigma, ET_A receptor antagonist) (2), L-NAME (1 mM, Sigma, St. Louis, MO and Tokyo, Japan, NOS inhibitor) (39), D-NAME (1 mM, Sigma, inactive enantiomer control), LY-83583 (or 6-anilino-5,8-quinolinedione, 10 μM, Biomol, Plymouth Meeting, PA, guanylate cyclase inhibitor) (39), and KT-5823 (2 μM, Sigma, specific cell-permeant cGMP-dependent protein kinase inhibitor) (16).

Transepithelial voltage (mV) was measured using the luminal perfusion pipette as an electrode. The voltage difference between calomel cells connected via 3 M KCl agar bridges to perfusate and bath was measured with a high-impedance electrometer.

Cell pH studies. Cell pH was measured by excitation ratio fluorometry (490 nm/445-nm excitation; 520-nm emission) using 5–10 μM BCECF (Molecular Probes, Eugene, OR) (26, 36). Fluorescence was detected in multiple intercalated cells and corrected for background (Photon Technology, London, Ontario). Movement and contaminating fluorescent signals were minimized by examining cells in focus close to the perfusion pipette and in the wall of the tubule. Duplicate readings were averaged in Burg's solution, after the reversible removal of luminal Cl^- and subsequently after the reversible removal of basolateral Cl^-. The sequence of readings was repeated in the same identified intercalated cells after 3-h incubation.

Agents were dissolved in 0.1% DMSO (vehicle) and added to the bathing solution 3–15 min before and during the 3-h incubation at pH 6.8. These agents included BQ-788 (1 μM, the ET_B receptor antagonist) and L-NAME (1 mM).

Statistics. Data are presented as means ± SE. Standard paired and unpaired comparisons were performed on spreadsheets using Excel 2003 (Microsoft, Bellvue, WA). One-way ANOVA, box plots, and post hoc Duncan and Scheffé's multiple comparison tests were used to examine the acid-incubated/basal H^+/HCO_3^- flux ratios and the acid-induced changes in net HCO_3^- flux using NCSS 6.0 statistical software (Kaysville, UT). Significance was asserted if $P < 0.05$ for each multiple comparison test.

RESULTS

Incubation at pH 6.8 induces a reversal in polarity of net HCO_3^- flux. To study the adaptation of intercalated cells, we utilized the model of in vitro acid incubation (21) and examined the effect of 3-h incubation of each CCD at pH 6.8 in both luminal and bathing solutions. In three CCDs taken from normal rabbits, the mean rate of bicarbonate transport before acid incubation was −3.18 ± 0.51 pmol·min^{-1}·mm^{-1}, indicating net HCO_3^- secretion. After 3-h incubation at pH 6.8, the solutions were restored to pH 7.4 and HCO_3^- transport was remeasured in the same tubule. After acid incubation the net flux was +3.07 ± 0.28 pmol·min^{-1}·mm^{-1} ($P < 0.05$), indicating net H^+ secretion, as has been shown previously (21). The transepithelial voltage became less negative after acid incubation, in keeping with a higher rate of net H^+ secretion (−2.9 ± 0.1 to −2.4 ± 0.1 mV, $P < 0.05$).

To dissect out the unidirectional fluxes of HCO_3^- and H^+ comprising the net flux, we incubated five CCDs at pH 6.8 and added a period in which luminal Cl^- was removed (and replaced by gluconate) to the pre- and postacid-incubation measurements. Bicarbonate transport in the absence of luminal Cl^- reflects the secretion of protons by α-intercalated cells, because HCO_3^- secretion is simultaneously inhibited in the β-intercalated cells. Figure 1 shows that the mean rate of net HCO_3^- transport was −3.81 ± 0.21 pmol·min^{-1}·mm^{-1}, which was comprised of an H^+ secretion rate of 3.69 ± 0.16 pmol·min^{-1}·mm^{-1} and a HCO_3^- secretion rate of −7.50 ± 0.36 pmol·min^{-1}·mm^{-1} (Table 1). After 3-h incubation at pH 6.8 in the presence of vehicle, the net HCO_3^- flux reversed polarity to net H^+ secretion (+3.27 ± 0.14 pmol·min^{-1}·mm^{-1}, $P < 0.01$); at 7.1 pmol·min^{-1}·mm^{-1} (Fig. 2), the change in net flux from basal to acid incubated was large enough to result in a change in

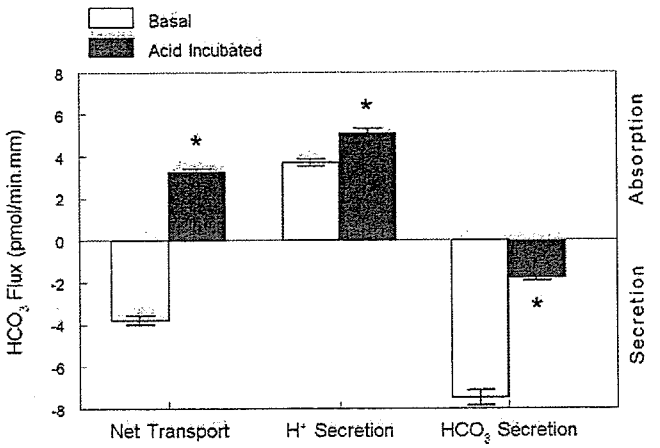

Fig. 1. Changes in H^+/HCO_3^- flux induced by incubation of cortical collecting duct (CCD) at pH 6.8 (n = 5 CCDs). *Left*: net bicarbonate transport. *Middle*: H^+ secretory fluxes obtained from luminal Cl^- removal (which inhibits HCO_3^- secretion). *Right*: HCO_3^- secretory fluxes obtained from the difference between the net and H^+ secretion flux. Each flux is presented before and following acid incubation. *Significantly different ($P < 0.01$) from basal value.

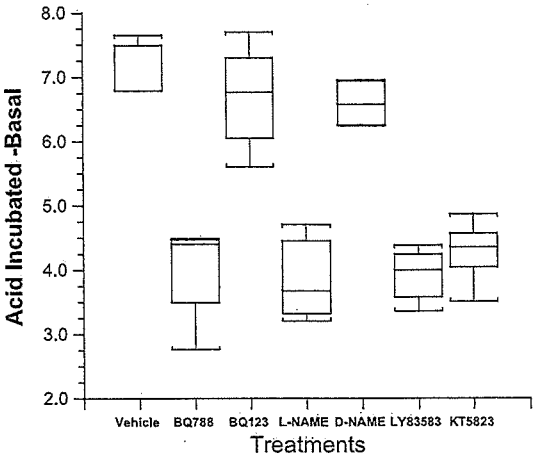

Fig. 2. Inhibition of ET_B receptor signaling blocks adaptive changes in net bicarbonate flux induced by acid incubation. The difference between acid-incubated and basal net bicarbonate flux in pmol·min^{-1}·mm^{-1} under various treatments is shown in box plots. Treatments include vehicle (n = 5), BQ-788 (n = 5), BQ-123 (n = 5), L-NAME (n = 4), D-NAME (n = 4), LY-83583 (n = 6), and KT-5823 (n = 6). The horizontal line represents the median, the *top* and *bottom* of the box represent the 75th and 25th percentiles, respectively, and the length of the box is the interquartile range; the T-shaped lines represent upper and lower adjacent values, wherein the former is the largest observation that is less than or equal to the 75th percentile plus 1.5 times the interquartile range and the latter is the smallest observation that is greater than or equal to the 25th percentile minus 1.5 times the interquartile range. The change in net bicarbonate flux is positive, indicating a shift from net secretion to zero net flux or to net HCO_3^- absorption. Because 1-way ANOVA was highly significant ($P < 0.001$), Duncan and Scheffé's multiple-comparison tests were performed. The change in vehicle net flux was significantly different from those due to BQ-788, L-NAME, LY-83583, and KT-5823, and the changes due to the inactive agents D-NAME and BQ-123 were also significantly different from these 4 treatments. The changes due to BQ-788, L-NAME, LY-83583, and KT-5823 were each significantly different from those due to vehicle, BQ-123, or D-NAME.

polarity from net HCO_3^- secretion to absorption. This adaptation was associated with a 39% increase in H^+ secretory flux to 5.08 ± 0.23 pmol·min^{-1}·mm^{-1} ($P < 0.05$; Table 1 and Fig. 3) and a 76% decrease in HCO_3^- secretory flux to −1.81 ± 0.11 pmol·min^{-1}·mm^{-1} ($P < 0.01$); the acid-incubated flux was 24% of the basal flux (Table 1 and Fig. 4). Concomitant with the increase in H^+ secretion, the transepithelial voltage tended to become less negative after acid incubation (−2.5 ± 0.1 to −2.1 ± 0.2 mV, P = 0.06).

Adaptive changes in H^+/HCO_3^- secretion fluxes induced by low pH are inhibited by ET_B receptor antagonism. Because ET secretion is induced by acidosis (42, 44) and ET receptor signaling regulates ion transport processes along the nephron (13, 32, 43), we examined the effect of ET receptor antagonism on the changes in H^+/HCO_3^- secretory fluxes induced by incubation at low pH. Acid incubation with BQ-788 failed to reverse the polarity of the net HCO_3^- flux (Table 1); that is, net HCO_3^- secretion was reduced to no significant HCO_3^- transport (−4.03 ± 0.29 to 0.047 ± 0.16 pmol·min^{-1}·mm^{-1}, $P <$ 0.01); at 4.1 pmol·min^{-1}·mm^{-1}, the change in net flux was significantly smaller than vehicle (Fig. 2). The reduction in net HCO_3^- secretion was not due to an offsetting increase in H^+ secretion [3.95 ± 0.10 to 4.05 ± 0.20, P = not significant (NS); Table 1 and Fig. 3, significantly smaller than vehicle], but rather to a 49% reduction in HCO_3^- secretion (−7.98 ± 0.35 to −4.00 ± 0.15 pmol·min^{-1}·mm^{-1}, $P < 0.01$); the acid-incubated HCO_3^- secretory flux was 51% of the basal flux (Table 1 and Fig. 4) and significantly larger than vehicle. The lack of change in H^+ secretion was associated with no significant change in transepithelial voltage (−2.13 ± 0.15 to −2.04 ± 0.14 mV, P = NS). BQ-123, an ET_A receptor

Table 1. *Basal and acid incubation net and H^+/HCO_3^- fluxes*

		Net Flux			H^+ Flux			HCO_3^- Flux		
Treatment	N	Basal	Acid	Δ	Basal	Acid	%	Basal	Acid	%
Vehicle	5	−3.8±0.21	3.3±0.14†	7.1	3.7±0.16	5.1±0.23*	39	−7.5±0.36	−1.8±0.11†	24
BQ-788	5	−4.0±0.29	0.1±0.16†	4.1	3.9±0.10	4.0±0.20	3	−8.0±0.35	−4.0±0.15†	51
BQ-123	5	−4.1±0.15	2.6±0.22†	6.7	3.5±0.18	4.9±0.22†	42	−7.6±0.26	−2.3±0.31†	30
L-NAME	4	−3.7±0.37	0.2±0.19†	3.8	3.2±0.06	3.9±0.08†	24	−6.8±0.38	−3.8±0.12†	56
D-NAME	4	−3.8±0.07	2.8±0.18†	6.6	3.6±0.19	4.9±0.22†	37	−7.4±0.22	−2.2±0.12†	29
LY-83583	6	−3.8±0.17	0.2±0.09†	3.9	3.2±0.11	3.8±0.18*	16	−7.0±0.27	−3.6±0.23†	51
KT-5823	6	−4.2±0.15	0.1±0.05†	4.3	3.6±0.12	4.0±0.12*	11	−7.9±0.22	−3.9±0.13†	50

Values are means ± SE. Fluxes are reported as pmol·min^{-1}·mm^{-1} tubule length; the fluxes have been rounded to 2 significant numbers to facilitate comparisons across the table. Δ Denotes change from basal to acid incubated, % denotes the ratio of acid-incubated/basal unidirectional H^+/HCO_3^- fluxes ×100. Concentrations of drug treatments were as follows: 1μM BQ-788 and 1–10μM BQ-123, D-NAME, 1 mM N^G-nitro-L-arginine methyl ester (L-NAME), 10 μM LY-83583, and 2 μM KT-5823. *Acid incubated significantly different from basal, $P < 0.05$. †Acid incubated significantly different from basal, $P < 0.01$.

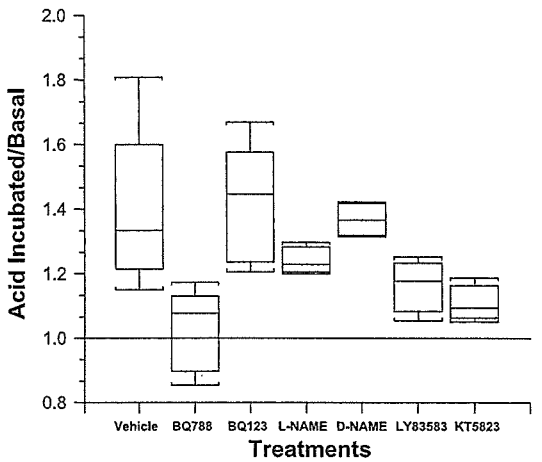

Fig. 3. Antagonism of ET_B receptor blocks increases in H^+ secretion induced by low pH. The ratio of acid-incubated/basal H^+ secretory fluxes under the various treatments is shown. The median and 75th and 25th percentiles are presented as in Fig. 2. The dashed horizontal line denotes the ratio of one, indicating no significant increase in H^+ secretion. ANOVA was highly significant ($P < 0.001$) and the multiple range comparisons showed that the vehicle was significantly different from BQ-788, LY-83583, and KT-5823. The H^+ secretory flux after BQ-788 treatment was significantly different from vehicle, L-NAME, D-NAME, and BQ-123; the BQ-788 ratio includes one within the interquartile range, indicating no significant increase in H^+ secretion with acid incubation. LY-83583 and KT-5823 treatments were significantly different from vehicle, D-NAME, and BQ-123.

antagonist used at 1–10 μM, did not prevent the changes in H^+ secretion and HCO_3^- secretion resulting from the incubation at pH 6.8. Acid incubation with BQ-123 resulted in a reversal of polarity of net HCO_3^- flux that was comparable to CCDs treated with vehicle control (Table 1 and Figs. 2–4). Because the response to acid incubation in the presence of BQ-788 resulted in a larger HCO_3^- secretory flux ($P < 0.05$) and a smaller H^+ secretory flux ($P < 0.05$) than in the presence of vehicle or BQ-123 incubation (Table 1 and Figs. 3 and 4), we concluded that ET_B, but not ET_A, receptor signaling was critical for the adaptation of the CCD to acidosis.

Time control. To ensure the stability of the isolated CCD preparation, we performed four timed control experiments with a 3-h incubation at pH 7.4; three of these experiments utilized 1 μM BQ-788 and the fourth used no inhibitor. Net bicarbonate secretion was unchanged by the incubation (or inhibitor): -3.89 ± 0.16 before and -3.83 ± 0.17 pmol·min^{-1}·mm^{-1} after incubation (P = NS). There was no change in H^+ secretory flux (3.44 ± 0.05 to 3.68 ± 0.21 pmol·min^{-1}·mm^{-1}, P = NS) or in HCO_3^- secretory flux (-7.33 ± 0.13 to -7.51 ± 0.29 pmol·min^{-1}·mm^{-1}, P = NS). In agreement with the stability of the H^+ secretory flux, there was no change in transepithelial voltage (-2.1 ± 0.1 to -2.1 ± 0.1 mV, P = NS). Similar data have been reported previously (33).

Adaptive decrease in HCO_3^- secretion flux induced by low pH requires NO synthesis. ET receptor signaling induces activation of NOS activity (9, 10). Therefore, we examined whether NO production was required for adaptation of the CCD to low pH. To detect the effect of NOS inhibition, we incubated five CCDs in 1 μM L-NAME just before and during the pH 6.8 incubation. Net HCO_3^- secretion before the acid incubation averaged -3.22 ± 0.22 pmol·min^{-1}·mm^{-1} and after acid incubation was only slightly greater than zero, 0.59 ± 0.02 pmol·min^{-1}·mm^{-1}. Whereas the change in net HCO_3^- flux was significant ($P < 0.01$), the acid-induced reversal of polarity of HCO_3^- flux was inhibited by L-NAME. When the inactive D-NAME was employed in two CCDs, the full adaptation and reversal of polarity of the net HCO_3^- flux were apparent (preincubation: -2.59 and -3.74 pmol·min^{-1}·mm^{-1}; postacid incubation: 2.94 and 2.79 pmol·min^{-1}·mm^{-1}, respectively).

We further examined the effect of NOS inhibition on the adaptation to low pH (in vitro acidosis) by measuring HCO_3^- transport in the presence and absence of luminal Cl^-. Table 1 shows that acid incubation with L-NAME resulted in a significant reduction, but not a reversal in polarity, of net HCO_3^- transport (-3.66 ± 0.37 to 0.16 ± 0.19 pmol·min^{-1}·mm^{-1}, $P < 0.01$); at 3.8 pmol·min^{-1}·mm^{-1}, the change in net flux was significantly smaller than vehicle (Fig. 2). This attenuated adaptation was associated with a 24% increase in H^+ secretory flux (3.17 ± 0.06 to 3.93 ± 0.08 pmol·min^{-1}·mm^{-1}, $P < 0.01$; Fig. 3) and a 44% decrease in HCO_3^- secretory flux (-6.84 ± 0.38 to -3.77 ± 0.12 pmol·min^{-1}·mm^{-1}, $P < 0.01$; Fig. 4); at 56%, the ratio of acid-incubated basal HCO_3^- secretory flux was significantly increased over vehicle, indicating a failure to adaptively reduce HCO_3^- secretion during acid incubation. The small increase in H^+ secretion was not associated with a significant decrease in transepithelial voltage (-2.3 ± 0.1 to -2.1 ± 0.2 mV, P = NS). In contrast, for CCDs incubated at pH 6.8 with the inactive enantiomer D-NAME, there was a complete adaptive reversal of polarity of net HCO_3^- flux (Table 1 and Figs. 2–4), similar to what was observed with vehicle control. These data show that NOS inhibition via L-NAME diminishes the downregulation of HCO_3^- secretion that occurs in response to incubation at low pH. L-NAME also partially blocks the acid-induced increase in H^+ secretion (24 vs. 37% for D-NAME; Table 1) but was not

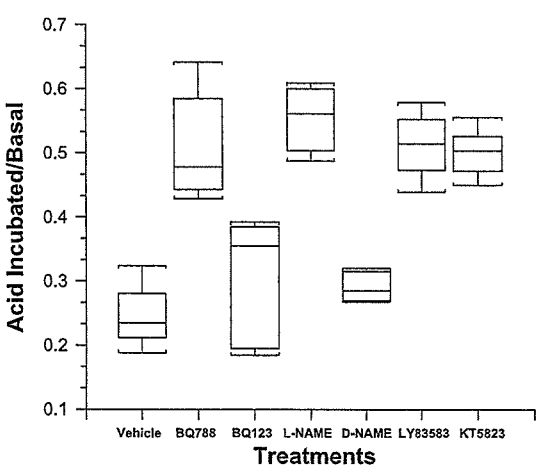

Fig. 4. Inhibition of ET_B receptor signaling blocks adaptive changes in HCO_3^- secretion induced by acid incubation. The ratio of acid-incubated/basal HCO_3^- secretory fluxes under the various treatments is shown. The median and 75th and 25th percentiles are presented as in Fig. 2. ANOVA was highly significant ($P < 0.001$) and the multiple range comparisons showed that vehicle was significantly different from BQ-788, L-NAME, LY-83583, and KT-5823 but was not different from D-NAME or BQ-123. D-NAME and BQ-123 were significantly different from BQ-788, L-NAME, LY-83583, and KT-5823. Each of the active treatments (BQ-788, L-NAME, LY-83583, and KT-5823) was significantly different from vehicle, BQ-123, and D-NAME.

as effective as the ET_B receptor antagonist, BQ-788 (Table 1 and Fig. 2), so that the end result is not a reversal in polarity of HCO_3^- transport, but a reduction to zero net transport.

ET_B receptor antagonism and L-NAME block the effect of acidosis on chloride-dependent cell pH changes. To confirm the changes in HCO_3^- transport, we examined β-intercalated cell pH changes in response to removal of Cl^- from the lumen or bath. Previously, we showed that β-intercalated cells express apical Cl^-/HCO_3^- exchangers and basolateral Cl^- conductances (21, 25). Figure 5*A* shows that when luminal Cl^- was removed, intercalated cell pH rose by 0.40 ± 0.04 pH U, but that after acid incubation, there was no alkalinization of cell pH with this maneuver (delta pH = −0.01 ± 0.03, $P <$ 0.01). When bath Cl^- was removed before the incubation, intercalated cell pH fell by −0.42 ± 0.01 pH U (Fig. 5*B*), but after acid incubation, the change in pH was reduced (delta pH = −0.18 ± 0.05, $P < 0.05$). Such an adaptation to reduce apical Cl^-/HCO_3^- exchange and basolateral Cl^- exit would be appropriate during metabolic acidosis.

BQ-788 added to the pH 6.8 incubation prevented the adaptive reduction in apical Cl^-/HCO_3^- exchange (0.46 ± 0.02 to 0.46 ± 0.01 pH U, P = NS; Fig. 5*C*) and in sensitivity to basolateral Cl^- removal (−0.44 ± 0.03 to −0.44 ± 0.04, P = NS; Fig. 5*D*). Similarly, L-NAME added to the pH 6.8 incubation clearly prevented the reduction in apical Cl^-/HCO_3^- exchange (0.47 ± 0.03 to 0.45 ± 0.03 pH U, P = NS; Fig. 5*E*) and in sensitivity to basolateral Cl^- removal (−0.48 ± 0.04 to −0.51 ± 0.05 pH U, P = NS; Fig. 5*F*). These results confirm that ET_B receptor signaling and NO synthesis are required for the adaptive decrease in HCO_3^- secretion (presumably by endocytosis of apical Cl^-/HCO_3^- exchangers) induced by incubation at low pH.

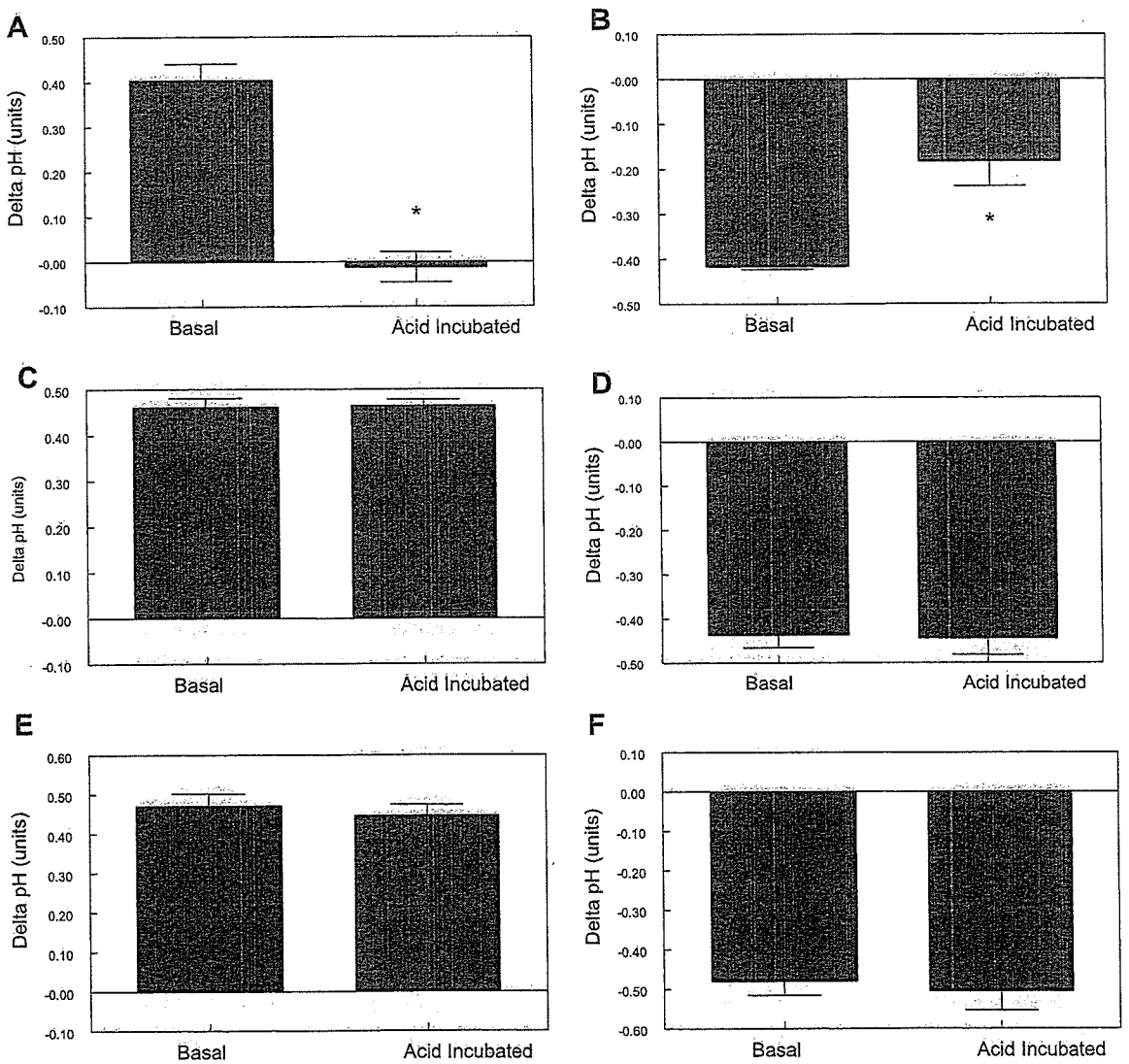

Fig. 5. ET_B receptor signaling is required for loss of luminal Cl^-/HCO_3^- exchange activity stimulated by low pH. Cell pH changes in response to Cl^- removal in basal state and after acid incubation are shown. *A*, *C*, and *E*: intercalated cell pH changes resulting from luminal Cl^- removal. *B*, *D*, and *F*: cell pH changes resulting from bath Cl^- removal. *A* and *B*: vehicle (n = 25 cells from 3 CCDs). *C* and *D*: BQ-788 (n = 40 cells from 5 CCDs). *E* and *F*: L-NAME (n = 66 cells from 7 CCDs). *Significantly different from basal value ($P < 0.01$).

cGMP generation and subsequent activation of PKG are required for acid-induced changes in H^+/HCO_3^- fluxes. Many of the effects of the signaling molecule NO are mediated by stimulation of NO-sensitive guanylate cyclase resulting in cGMP formation and the subsequent activation of cGMP-dependent protein kinase (PKG) (7, 15). We tested the effect on HCO_3^- transport of 10 μM LY-83583, an inhibitor of soluble guanylate cyclase, during acid incubation (Fig. 2). LY-8353 markedly attenuated the reversal of polarity of net HCO_3^- flux in response to low pH, and there was no net HCO_3^- flux (-3.76 ± 0.17 to 0.18 ± 0.09 pmol·min^{-1}·mm^{-1}, $P < 0.01$; Table 1); at 3.9 pmol·min^{-1}·mm^{-1}, the difference between acid-incubated and basal net flux was much smaller than vehicle or inactive agent (D-NAME or BQ-123, Table 1 and Fig. 2). There was a only a 16% increase in H^+ secretion, smaller than seen with vehicle or inactive agent (3.25 ± 0.11 to 3.79 ± 0.17 pmol·min^{-1}·mm^{-1}, $P < 0.05$; Table 1 and Fig. 3), and a 49% reduction in HCO_3^- secretion (-7.01 ± 0.27 to -3.60 ± 0.23 pmol·min^{-1}·mm^{-1}, $P < 0.01$), such that at 51% the ratio of acid-incubated/basal HCO_3^- secretory flux was significantly increased compared with vehicle or inactive agent (Fig. 4). The increase in acid/basal H^+ secretion and the decrease in acid/basal HCO_3^- secretion were smaller than those observed after acid incubation with vehicle ($P < 0.05$; Table 1).

The role of PKG in the acid-induced adaptation was tested by examining the effect of 2 μM KT-5823, a specific cell-permeant inhibitor of PKG, on H^+/HCO_3^- fluxes. KT-5823 substantially prevented the reversal of polarity of HCO_3^- flux in response to low pH, so that there was no net flux after acid incubation (-4.22 ± 0.15 to 0.08 ± 0.05 pmol·min^{-1}·mm^{-1}, $P < 0.01$; Table 1); at 4.3 pmol·min^{-1}·mm^{-1}, the change in net flux from basal to acid incubated was significantly smaller than vehicle or inactive controls (Fig. 2). The increase in acid/basal H^+ secretion and the decrease in acid/basal HCO_3^- secretion were smaller than those observed after acid incubation with vehicle or inactive controls ($P < 0.05$; Table 1 and Figs. 3 and 4). These results suggest that inhibitors of guanylate cyclase and PKG partially prevent the adaptive increase in H^+ secretion and the decrease in HCO_3^- secretion that would be anticipated in response to metabolic acidosis.

Taken together, these data indicate that the adaptive decrease in HCO_3^- secretion in response to acidosis is mediated in large part by ET-ET_B-NO-guanylate cyclase-PKG signaling pathway. In contrast, the adaptive increase in H^+ secretion, which may be directly stimulated by ET-ET_B signaling, tends to be less affected by the NO-signaling pathway.

DISCUSSION

To investigate the role of ET and NO in intercalated cells of the CCD, we made use of our in vitro acidosis model in which incubation of a CCD for 3 h at pH 6.8 induces a change in polarity of net HCO_3^- flux from net secretion to net absorption (21, 26). This model recapitulates the pathophysiological condition of 3 days of NH_4Cl loading (in the drinking water) that results in metabolic acidosis in vivo (21, 25). The adaptation to acid treatment is accomplished by two adjustments: increased H^+ secretion, presumably by existing and perhaps recruited α-intercalated cells, and decreased HCO_3^- secretion by β-intercalated cells (23, 24, 33). The rabbit CCD contains both α- and β-intercalated cells, and both types are active under normal conditions. Previously, we showed that luminal bafilomycin, by inhibiting the apical H^+-ATPase of α-intercalated cells of CCDs from normal rabbits, reduces H^+ secretion and thereby makes the net HCO_3^- flux more negative (higher rate of secretion under basal conditions). When bafilomycin was used after acid incubation, the basal and adaptive increases in H^+ secretion were inhibited, such that net HCO_3^- transport was not significantly different from zero (33). The effect of inhibiting the H^+-K^+-ATPase was previously shown (33) to be much smaller than that of inhibiting the H^+-ATPase in acid-adapted CCDs, indicating a limited role for the H^+-K^+-ATPase in adapting to metabolic acidosis. These data show that there is a substantial amount of HCO_3^- secretion in CCDs from normal rabbits, but after they are incubated at low pH, the HCO_3^- secretion rate is greatly diminished, such that when the offsetting H^+ secretion by α-intercalated cells is inhibited by bafilomycin, there is virtually no net HCO_3^- transport. These data also show that there are partially offsetting H^+ secretory fluxes in CCDs from normal rabbits but after acid incubation, the basal and adaptive increase in H^+ secretion are entirely inhibited by a vacuolar H^+-ATPase inhibitor. In this study, we extended these observations by demonstrating that ET_B receptor signaling in response to low pH mediated the decreased HCO_3^- secretion as well as the adaptive increase in H^+ secretion. It is not surprising that the ET_B receptor antagonist entirely inhibited the adaptive increase in H^+ secretion, because Wesson's group showed inhibition of B- but A-type ET receptors blunts not only the decreased HCO_3^- secretion but also the increased H^+ secretion in the distal tubule of rats given dietary acid (42). Thus ET, via the ET_B receptor, regulates adaptive changes in H^+/HCO_3^- fluxes during metabolic acidosis.

NO has been found to play an important role in mediating salt and water transport, in addition to hemodynamics and tubuloglomerular feedback in the kidney (17). Less is known about how NO affects acid-base transport. Mice lacking nNOS have defective proximal tubule HCO_3^- reabsorption and develop metabolic acidosis (41). Mice lacking inducible NOS, but not endothelial NOS, also show reduced proximal HCO_3^- reabsorption (40). These studies show that inducible and nNOS stimulate proximal HCO_3^- reabsorption. Also, acidosis stimulates NO synthesis in rat lung (18) and canine heart (11), perhaps because the cellular acidosis increases cellular calcium levels (4, 38), and calcium activates NOS (15).

The CCD is known to express endothelial, inducible, and nNOS (1, 14, 30, 31, 37) and NO has important actions in the CCD. NO inhibits ADH-stimulated osmotic water permeability in the CCD (5, 6). Also, in M-1 cultured CCD cells, NO inhibits sodium transport at the apical membrane sodium channel (27). The present study adds modulation of β-intercalated cell HCO_3^- secretory fluxes in response to acidosis to the actions of NO on ion transport in the CCD. There are no reports of NO stimulating H^+ secretion in the CCD; and furthermore, results of this study fail to demonstrate a pivotal role for NO guanylate cyclase in upregulating H^+ secretion. However, Tojo et al. (31) showed that exogenous donors of NO inhibit bafilomycin-sensitive H^+-ATPase activity in microdissected rat CCDs, suggesting that an inducible form of NOS downregulates H^+ secretion by α-intercalated cells. It is possible that ET-ET_B signaling to control H^+ secretion works via another pathway that predominates over the NO-guanylate cyclase system.

Activation of soluble guanylate cyclase leading to the production of cGMP is a key function of NO as a signal generator. cGMP has several targets, with the major one being PKG (7). cGMP has recently been shown to cause the membrane insertion of aquaporin-2 in renal epithelial cells (3). Results presented in the present study demonstrate that activation of guanylate cyclase and subsequent stimulation of PKG are critical for the adaptation of the β-intercalated cell to acidosis. Based on the analysis of HCO_3^- flux and cell pH changes in response to luminal Cl^- removal, we suggest that cGMP activation of PKG stimulates endocytosis of apical Cl^-/HCO_3^- exchangers, leading to a decrease in HCO_3^- secretion in response to acidosis. Identification of substrates of PKG that directly or indirectly influence endocytic pathways is an important area for further investigation.

GRANTS

This work was supported in part by a Grant-in-Aid from the American Heart Association (0455829T) New York State Affiliate (G. J. Schwartz) and by grants from the Ministry of Education, Culture, Sports, Science and Technology, and Ministry of Health, Labor and Welfare of Japan (S. Tsuruoka).

REFERENCES

1. **Ahn KY, Mohaupt MG, Madsen KM, and Kone BC.** In situ hybridization localization of mRNA encoding inducible nitric oxide synthase in rat kidney. *Am J Physiol Renal Fluid Electrolyte Physiol* 267: F748–F757, 1994.
2. **Bhowmick N, Narayan P, and Puett D.** The endothelin subtype A receptor undergoes agonist- and antagonist-mediated internalization in the absence of signaling. *Endocrinology* 139: 3185–3192, 1998.
3. **Bouley R, Breton S, Sun T, McLaughlin M, Nsumu NN, Lin HY, Ausiello DA, and Brown D.** Nitric oxide and atrial natriuretic factor stimulate cGMP-dependent membrane insertion of aquaporin 2 in renal epithelial cells. *J Clin Invest* 106: 1115–1126, 2000.
4. **Cannon C, van Adelsberg J, Kelly S, and Al-Awqati Q.** Carbon-dioxide-induced exocytotic insertion of H^+ pumps in turtle bladder luminal membrane: role of cell pH and calcium. *Nature* 314: 443–446, 1985.
5. **Garcia NH, Pomposiello SI, and Garvin JL.** Nitric oxide inhibits ADH-stimulated osmotic water permeability in cortical collecting ducts. *Am J Physiol Renal Fluid Electrolyte Physiol* 270: F206–F210, 1996.
6. **Garcia NH, Stoos BA, Carretero OA, and Garvin JL.** Mechanism of the nitric oxide-induced blockade of collecting duct water permeability. *Hypertension* 27: 679–683, 1996.
7. **Hanafy KA, Krumenacker JS, and Murad F.** NO, nitrotyrosine, and cyclic GMP in signal transduction. *Med Sci Monit* 7: 801–819, 2001.
8. **Hercule HC and Oyekan AO.** Cytochrome P450 omega/omega-1 hydroxylase-derived eicosanoids contribute to endothelin(A) and endothelin(B) receptor-mediated vasoconstriction to endothelin-1 in the rat preglomerular arteriole. *J Pharmacol Exp Ther* 292: 1153–1160, 2000.
9. **Herrera M and Garvin JL.** Endothelin stimulates endothelial nitric oxide synthase expression in the thick ascending limb. *Am J Physiol Renal Physiol* 287: F231–F235, 2004.
10. **Hirata Y, Emori T, Eguchi S, Kanno K, Imai T, Ohta K, and Marumo F.** Endothelin receptor subtype B mediates synthesis of nitric oxide by cultured bovine endothelial cells. *J Clin Invest* 91: 1367–1373, 1993.
11. **Kitakaze M, Node K, Takashima S, Asanuma H, Asakura M, Sanada S, Shinozaki Y, Mori H, Sato H, Kuzuya T, and Hori M.** Role of cellular acidosis in production of nitric oxide in canine ischemic myocardium. *J Mol Cell Cardiol* 33: 1727–1737, 2001.
12. **Kohan DE.** Endothelin synthesis by rabbit renal tubule cells. *Am J Physiol Renal Fluid Electrolyte Physiol* 261: F221–F226, 1991.
13. **Laghmani K, Preisig PA, Moe OW, Yanagisawa M, and Alpern RJ.** Endothelin-1/endothelin-B receptor-mediated increases in NHE3 activity in chronic metabolic acidosis. *J Clin Invest* 107: 1563–1569, 2001.
14. **Mohaupt MG, Elzie JL, Ahn KY, Clapp WL, Wilcox CS, and Kone BC.** Differential expression and induction of mRNAs encoding two inducible nitric oxide synthases in rat kidney. *Kidney Int* 46: 653–665, 1994.
15. **Moncada S and Higgs A.** The L-arginine-nitric oxide pathway. *N Engl J Med* 329: 2002–2012, 1993.
15a. **Ohuchi T, Yanagisawa M, and Gariepy CE.** Renal tubular effects of endothelin-B receptor signaling: its role in cardiovascular hemeostasis and extracellular volume regulation. *Curr Opin Nephrol Hypertens* 9: 435–439, 2000.
16. **Ortiz PA and Garvin JL.** Autocrine effects of nitric oxide on HCO_3^- transport by rat thick ascending limb. *Kidney Int* 58: 2069–2074, 2000.
17. **Ortiz PA and Garvin JL.** Role of nitric oxide in the regulation of nephron transport. *Am J Physiol Renal Physiol* 282: F777–F784, 2002.
18. **Pedoto A, Caruso JE, Nandi J, Oler A, Hoffmann SP, Tassiopoulos AK, McGraw DJ, Camporesi EM, and Hakim TS.** Acidosis stimulates nitric oxide production and lung damage in rats. *Am J Respir Crit Care Med* 159: 397–402, 1999.
19. **Plato CF, Pollock DM, and Garvin JL.** Endothelin inhibits thick ascending limb chloride flux via ET_B receptor-mediated NO release. *Am J Physiol Renal Physiol* 279: F326–F333, 2000.
20. **Plato CF, Stoos BA, Wang D, and Garvin JL.** Endogenous nitric oxide inhibits chloride transport in the thick ascending limb. *Am J Physiol Renal Physiol* 276: F159–F163, 1999.
21. **Satlin LM and Schwartz GJ.** Cellular remodeling of HCO_3^--secreting cells in rabbit renal collecting duct in response to an acidic environment. *J Cell Biol* 109: 1279–1288, 1989.
22. **Schnermann J, Lorenz JN, Briggs JP, and Keiser JA.** Induction of water diuresis by endothelin in rats. *Am J Physiol Renal Fluid Electrolyte Physiol* 263: F516–F526, 1992.
23. **Schuster VL.** Function and regulation of collecting duct intercalated cells. *Annu Rev Physiol* 55: 267–288, 1993.
24. **Schwartz GJ.** Plasticity of intercalated cell polarity: effect of metabolic acidosis. *Nephron* 87: 304–313, 2001.
25. **Schwartz GJ, Barasch J, and Al-Awqati Q.** Plasticity of functional epithelial polarity. *Nature* 318: 368–371, 1985.
26. **Schwartz GJ, Tsuruoka S, Vijayakumar S, Petrovic S, Mian A, and Al-Awqati Q.** Acid incubation reverses the polarity of intercalated cell transporters, an effect mediated by hensin. *J Clin Invest* 109: 89–99, 2002.
27. **Stoos BA, Carretero OA, and Garvin JL.** Endothelial-derived nitric oxide inhibits sodium transport by affecting apical membrane channels in cultured collecting duct cells. *J Am Soc Nephrol* 4: 1855–1860, 1994.
28. **Takemoto F, Uchida S, Ogata E, and Kurokawa K.** Endothelin-1 and endothelin-3 binding to rat nephrons. *Am J Physiol Renal Fluid Electrolyte Physiol* 264: F827–F832, 1993.
29. **Terada Y, Tomita K, Nonoguchi H, and Marumo F.** Polymerase chain reaction localization of constitutive nitric oxide synthase and soluble guanylate cyclase messenger RNAs in microdissected rat nephron segments. *J Clin Invest* 90: 659–665, 1992.
30. **Tojo A, Guzman NJ, Garg LC, Tisher CC, and Madsen KM.** Nitric oxide inhibits bafilomycin-sensitive H^+-ATPase activity in rat cortical collecting duct. *Am J Physiol Renal Fluid Electrolyte Physiol* 267: F509–F515, 1994.
31. **Tomita K, Nonoguchi H, Terada Y, and Marumo F.** Effects of ET-1 on water and chloride transport in cortical collecting ducts of the rat. *Am J Physiol Renal Fluid Electrolyte Physiol* 264: F690–F696, 1993.
32. **Tsuruoka S and Schwartz GJ.** Adaptation of rabbit cortical collecting duct HCO_3^- transport to metabolic acidosis in vitro. *J Clin Invest* 97: 1076–1084, 1996.
33. **Tsuruoka S and Schwartz GJ.** Metabolic acidosis stimulates H^+ secretion in the rabbit outer medullary collecting duct (inner stripe) of the kidney. *J Clin Invest* 99: 1420–1431, 1997.
34. **Tsuruoka S, Schwartz GJ, Wakaumi M, Nishiki K, Yamamoto H, Purkerson JM, and Fujimura A.** Nitric oxide production modulates cyclosporin A-induced distal renal tubular acidosis in the rat. *J Pharmacol Exp Ther* 305: 840–845, 2003.
35. **Tsuruoka S, Swenson ER, Petrovic S, Fujimura A, and Schwartz GJ.** Role of basolateral carbonic anhydrase in proximal tubular fluid and bicarbonate absorption. *Am J Physiol Renal Physiol* 280: F146–F154, 2001.
36. **Ujiie K, Yuen J, Hogarth L, Danziger R, and Star RA.** Localization and regulation of endothelial NO synthase mRNA expression in rat kidney. *Am J Physiol Renal Fluid Electrolyte Physiol* 267: F296–F302, 1994.
37. **Van Adelsberg J and Al-Awqati Q.** Regulation of cell pH by Ca^{2+}-mediated exocytotic insertion of H^+-ATPases. *J Cell Biol* 102: 1638–1645, 1986.

39. **Wang H, Carretero OA, and Garvin JL.** Nitric oxide produced by THAL nitric oxide synthase inhibits TGF. *Hypertension* 39: 662–666, 2002.
40. **Wang T.** Role of iNOS and eNOS in modulating proximal tubule transport and acid-base balance. *Am J Physiol Renal Physiol* 283: F658–F662, 2002.
41. **Wang T, Inglis FM, and Kalb RG.** Defective fluid and HCO_3^- absorption in proximal tubule of neuronal nitric oxide synthase-knockout mice. *Am J Physiol Renal Physiol* 279: F518–F524, 2000.
42. **Wesson DE.** Endogenous endothelins mediate increased distal tubule acidification induced by dietary acid in rats. *J Clin Invest* 99: 2203–2211, 1997.
43. **Wesson DE and Dolson GM.** Endothelin-1 increases rat distal tubule acidification in vivo. *Am J Physiol Renal Physiol* 273: F586–F594, 1997.
44. **Wesson DE, Simoni J, and Green DF.** Reduced extracellular pH increases endothelin-1 secretion by human renal microvascular endothelial cells. *J Clin Invest* 101: 578–583, 1998.
45. **Yanagisawa M, Kurihara H, Kimura S, Tomobe Y, Kobayashi M, Mitsui Y, Yazaki Y, Goto K, and Masaki T.** A novel potent vasoconstrictor peptide produced by vascular endothelial cells. *Nature* 332: 411–415, 1988.
46. **Yasoshima K, Satlin LM, and Schwartz GJ.** Adaptation of rabbit cortical collecting duct to in vitro acid incubation. *Am J Physiol Renal Fluid Electrolyte Physiol* 263: F749–F756, 1992.

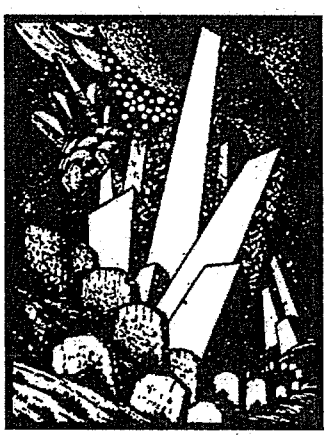

Journal of Environmental Biotechnology
Vol. 6, No. 1, 41–46, 2006

Original paper (regular paper)

Polyamines Affect Polyphosphate Accumulation in *Escherichia coli*

KEI MOTOMURA[1], NOBORU TAKIGUCHI[1], HISAO OHTAKE[2] and AKIO KURODA[1,3]*

[1] *Department of Molecular Biotechnology, Hiroshima University, Hiroshima 739-8530, Japan*
[2] *Department of Biotechnology, Osaka University, Osaka 565-0871, Japan*
[3] *SORST, Japan Science and Technology Corporation, Kawaguchi, Saitama 332-0012, Japan*
* TEL: 082–424–7758 FAX: 082–424–7047
* E-mail: akuroda@hiroshima-u.ac.jp

(Received; 4 April, 2006/Accepted; 1 May, 2006)

In the current studies, we showed that a *speABC* and *cadA* mutant of *Escherichia coli*, which fails to produce polyamines such as putrescine, spermidine, and cadaverine, accumulates reduced levels of polyphosphate (polyP) under conditions of amino acid starvation. This was reversed by supplementation of the culture medium with polyamines. In addition, a *speG* mutant, which accumulates polyamines, increased levels of polyP, suggesting that polyamines affect polyP accumulation. Although polyP granules are often found in cellular inclusions containing calcium, those isolated from *E. coli* did not contain calcium. We found that these polyP granules soon disappear when they are placed in a buffer but that they are stabilized by the presence of polyamines. We concluded that polyamines interact with polyP and affect polyP accumulation.

Key words: Polyphosphate, polyamine, *Escherichia coli*, polyphosphate granule

1. Introduction

Increased input of inorganic phosphate (P_i) into lakes, bays, and other surface waters causes the nuisance growth of phytoplankton, called an algal bloom[6]. Hence, considerable attention has been paid to efficient removal of P_i from wastewater[6,28]. In traditional sewage works, 20% to 40% of P_i in wastewater is typically removed in the sludge by biological conversion to organic phosphate such as DNA, RNA, and phospholipid. Improvement of the ability to accumulate phosphorus compounds in the sludge should therefore help in the removal of P_i from wastewater.

Inorganic polyphosphate (polyP) is a linear polymer of many tens or hundreds of P_i molecules connected by high-energy bonds[14,15]. PolyP is found in a wide range of prokaryotes and eukaryotes[14,15]. PolyP has various biological functions, for example, as a P_i reservoir[14,15], an alternative source of high-energy bonds[14,15], as a buffer against alkaline conditions and metal accumulation[23], and as a regulator for transcription[14] and proteolysis[18]. PolyP has an osmotic advantage over free P_i for accumulation of phosphorus in cells. Therefore, enhanced biological phosphorus removal is based on the use of bacteria capable of accumulating polyP.

PolyP kinase (PPK), a tetramer of 80-kDa subunits, is responsible for the processive synthesis of long-chain polyP (750 P_i residues) in *Escherichia coli*[14]. PPK catalyzes the reversible reaction of the γ-terminal P_i of ATP to polyP[14]. So far, *phoU*, *spoT*, and *relA* genes have been identified as regulators of polyP accumulation[16,21]. A *phoU* mutant, which derepresses the phosphate regulon, accumulates polyP[21]. Constitutive expression of the PstSCAB P_i uptake system in the *phoU* mutants is responsible for the elevated levels of polyP[21]. On the other hand, the level of polyP in *E. coli* is very low during the exponential phase but increases up to 1000-fold in response to amino acid starvation[16]. An *E. coli relA spoT* mutant that fails to produce guanosine penta- and tetra-phosphate (pppGpp and ppGpp) is deficient in the accumulation of polyP in response to amino acid starvation[16]. It was found that the stringent factors pppGpp and ppGpp strongly inhibit polyphosphatase PPX[16]. PPK and PPX activities are constitutively expressed, but when pppGpp and ppGpp build up in the cells during amino acid starvation, polyP may accumulate due to inhibition of PPX.

Polyamines, polycationic compounds present in all living organisms, have been implicated in a wide variety of biological reactions, including nucleic acid and protein synthesis[3,10]. Polyamines are thought to participate in these cellular processes through binding to DNA and RNA[10,11]. Polyamine content is regulated by its biosynthesis, degradation, uptake, and excretion[9,22]. A polyamine-deficient strain of *E. coli* has been obtained as a result of deletions in *speA* (arginine decarboxylase), *speB* (agmatine ureohydrolase), *speC* (ornithine decarboxylase), and *cadA* (cadavarine biosynthesis)[13,29]. Although this strain lacks putrescine, spermidine, and cadaverine, it is still able to slowly but indefinitely grow on polyamine-deficient media[13,29]. In the presence of polyamines in the medium, an *speABC* and *cadA* mutant can take up polyamines and grow well. On the other hand, a spermidine acetyltransferase gene (*speG*) mutant that fails

to degrade polyamine accumulates approximately 3-fold higher levels of spermidine when grown in a medium containing spermidine[5]. We speculated that polyamines interact not only with DNA and RNA but also polyP, and we demonstrated that polyamines affect polyP accumulation under conditions of amino acid starvation.

2. Materials and Methods

2.1. Plasmid construction

A 2.6-kb *Kpn*I fragment containing *ppk* of pBC10 was inserted into the *Kpn*I site of pMW119. The orientation of the *ppk* insertion in the resulting plasmid pMWppk was opposite the lac promoter of pMW119[17].

2.2. Bacterial strains and growth conditions

E. coli speABC, *cadA*, and *speG* mutants were constructed according to the one-step gene inactivation method described by Datsenko and Wanner[4]. First, DNA fragments containing target and antibiotic genes were prepared by polymerase chain reaction using the primers listed in Table 1. These DNA fragments were then introduced into *E. coli* and replaced with the chromosomal genes. The *speABC cadA* mutant was grown in a 2xYT rich medium (1.6% peptone, 1.0% yeast extract, and 0.5% NaCl) with shaking at 37°C for 12–18 h. This culture was diluted in a MOPS-minimal medium (22.2 mM glucose, 40 mM potassium morpholinopropane sulfonate [pH 7.2], 50 mM NaCl, 9.52 mM NH_4Cl, 4 mM Tricine, 2 mM K_2HPO_4, 0.52 mM $MgCl_2$, 0.28 mM K_2SO_4, 0.01 mM $FeSO_4$, 0.0005 mM $CaCl_2$, and trace metals)[17] containing 2% casamino acid and 0.4 M sorbitol and then cultivated overnight. To deplete endogenous polyamines, this cultivation was repeated, and the culture was inoculated into the MOPS-minimal medium containing 2% casamino acid and 0.4M sorbitol. The fresh medium was supplemented with 1 mM putrescine and spermidine as necessary. After a 6-h incubation, the *E. coli speABC cadA* mutant was collected by centrifugation. The cell pellet was washed once with the MOPS-minimal medium containing 0.4 M sorbitol and resuspended in the same medium (amino acid-starved condition). The *E. coli speG* mutant was grown to mid-log phase in the 2xYT medium with shaking at 37°C and shifted to the MOPS-minimal medium. PolyP granules were observed under fluorescent microscopy (BX-50, Olympus) after staining with 4',6-diamidino-2-phenylindole (DAPI). PolyP was recovered with silicate glass from cells lysed with guanidine isothiocyanate and determined by a two-enzyme assay[1].

2.3. Preparation of polyP granules from *E. coli*

The *E. coli phoU* mutant was grown to mid-log phase in the 2xYT medium with shaking at 37°C and shifted to the MOPS-minimal medium for 2 h to cause the accumulation of a large amount of polyP-containing granules[21]. PolyP granules were prepared essentially as described by Jacobson[12]. Freeze-dried cells (0.1 g), zirconia beads (diameter 2 mm; 3.5 g), and carbon tetrachloride (400 µl) were mixed in a 2-ml tube. The suspension was homogenized twice for 30 s using a Micro Smash (Tomy, Tokyo, Japan) at a speed of 4000 rpm in a cold room. PolyP granules were precipitated by centrifugation at 13,000×*g* for 10 min. The cell debris was not precipitated under this condition. The pellet containing polyP granules was washed several times with carbon tetrachloride and dried. PolyP granules were observed by scanning electron microscopy, and their chemical composition was analyzed by electron microscopy coupled with energy-dispersive X-ray spectroscopy (EDAX; Nihon Denshi).

2.4. *In vitro* preparation of polyP granules

PolyP granules were formed by mixing 50 mM polyP (average chain-length=65; Sigma), 57 mM KCl, and 39 mM $MgCl_2$. PolyP granules were collected by centrifugation at 13,000×*g* for 5 min and washed five times with a solution containing 57 mM KCl and 39 mM $MgCl_2$.

Table 1. Primers used for gene disruption.

Gene	DNA sequence
speAB	ACTGTTTTACACTTAATAAAATAATTTGAGGTTCGCTATGATTCC-GGGGATCCGTCGACC (forward)
	TGCGCATCGCATCTGGTGCTTACTCGCCCTTTTTCGCCGCTGTAG-GCTGGAGCTGCTTCG (reverse)
speC	GGCGGTCGGAGCTGGTGACCAGTTTGACCCATATCTCATGATTCC-GGGGATCCGTCGACC (forward)
	TGACCCGTTTTTTTTATTCTTACTTCAACACATAACCGTATGTAG-GCTGGAGCTGCTTCG (reverse)
cadA	GTGTTGGGAGGGGCCTTTTTTACCTGGAGATATGACTATGATTCC-GGGGATCCGTCGACC (forward)
	CTTCCCTTGTACGAGCTAATTATTTTTTGCTTTCTTCTTTTTGTAG-GCTGGAGCTGCTTCG (reverse)
speG	TAACCTGTTATTGATTTAAGGAATGTAAGGACACGTTATGATTCC-GGGGATCCGTCGACC (forward)
	CGATCGATTATTATTAATGCTATTGTGCGGTCGGCTTCAGTGTAG-GCTGGAGCTGCTTCG (reverse)

2.5. Stability of polyP granules

PolyP granules prepared *in vitro* were dispersed in 100 mM sodium hydroxyetylpiperazine ethanesulphonate (HEPES-NaOH, pH 7.2) containing each polyamine (putrescine, spermidine, cadaverine), or ammonium chloride at room temperature. After the indicated time, polyP granules were precipitated at 13,000×*g* for 3 min. PolyP was determined as P_i by the ascorbic acid method after hydrolysis in 1 N HCl at 100°C for 7 min[2,7].

3. Results and Discussion

3.1. Polyamines affect polyP accumulation in *E. coli*

PolyP accumulated in response to amino acid starvation in *E. coli* (Fig. 1A). PolyP is a P_i polymer with some similarity to RNA and DNA, and, therefore, it is reasonable that polyP readily interacts with polycationic compounds including polyamines. To determine whether polyamines affect polyP accumulation under conditions of amino acid starvation, we constructed a *speABC* and *cadA* mutant that fails to produce polyamines[13,29]. The intracellular levels of polyamines in this mutant can be restored by the addition of polyamines to the medium. The levels of polyP in this mutant were also partially restored by addition of polyamines to the medium under conditions of amino acid starvation (Fig. 1A). In addition, introduction of a low-copy plasmid encoding *ppk* (pMWppk) increased the levels of polyP. Under conditions of amino acid starvation, an *speABC* and *cadA* mutant carrying pMWppk accumulated more polyP in the presence than in the absence of polyamines in the medium (Fig. 1B). On the other hand, accumulation of polyamines by a *speG* mutant was enhanced three-fold by the addition of polyamines to the medium.

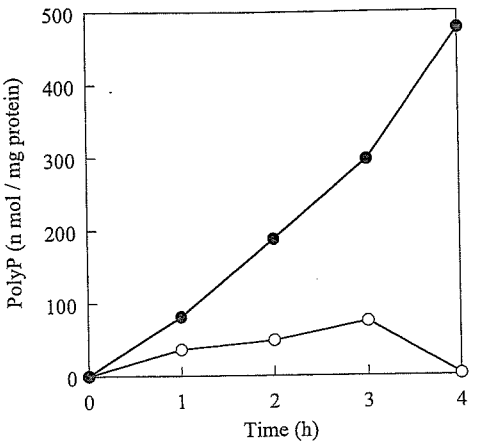

Fig. 2. PolyP accumulation in a *speG* mutant and the wild type under conditions of amino acid starvation in the presence of polyamines.
Intracellular polyP concentrations were measured for *E. coli* MG1655 (open circles) and a *speG* mutant (closed circles) at the indicated times after shifting to MOPS medium containing polyamines (1 mM putrescine and 1 mM spermidine).

This mutant also accumulated more polyP than the wild type (Fig. 2). After 3 h, the wild type restarted to grow under this condition and its polyP accumulation reduced (Fig. 2). However, this mutant could not adapt to amino acid starvation and thus polyP accumulation might prolong even after 3 h. These results suggested that polyamines affect polyP accumulation.

3.2. Analysis of polyP granules prepared from *E. coli*

PolyP is often found in cellular inclusions known as polyP granules or volutin granules[19,25,26,27]. Here, we isolated polyP granules from an *E. coli phoU* mutant that accumulates 1000-fold higher levels of polyP than the wild type.

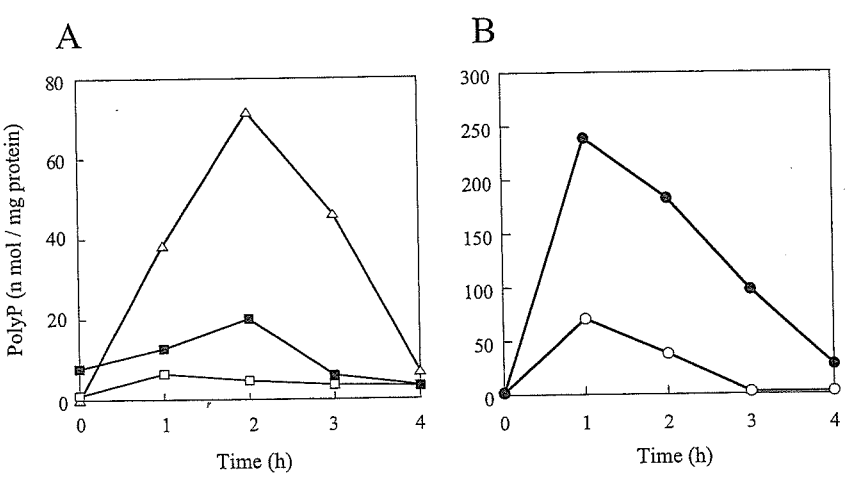

Fig. 1. PolyP accumulation in a *speABC cadA* mutant under conditions of amino acid starvation and in the presence and absence of polyamines.
(A) Intracellular polyP concentrations were measured in the *E. coli* wild type at the indicated times after shifting to amino acid-starved conditions (open triangles). The polyP concentrations were also measured in an *E. coli speABC cadA* mutant at the indicated times after shifting to amino acid-starved conditions with (closed squares) or without (open squares) added polyamines (1 mM putrescine and 1 mM spermidine). (B) The same experiment was performed in the *E. coli speABC cadA* mutant carrying pMWppk in the presence (closed circular) or absence (open circular) of polyamines.

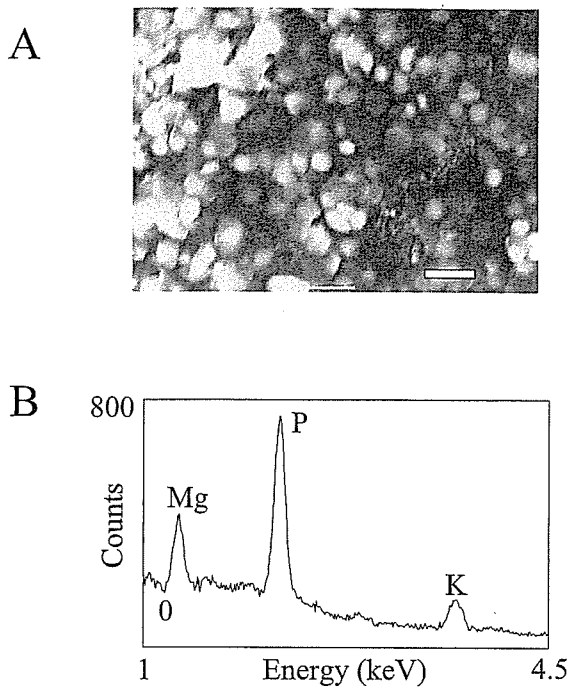

Fig 3. Scanning electron microscopy (A) and EDAX spectra (B) of polyP granules prepared from *E. coli* cells.
(A) PolyP granules extracted from *E. coli* with carbon tetrachloride were evaporated on the stage, coated with carbon, and then observed by scanning electron microscopy. Bar=2 μm. (B) The elemental composition of polyP granules was analyzed by EDAX.

We examined the polyP granules by microscopy and by scanning electron microscopy with EDAX (Fig. 3). EDAX analysis revealed that polyP granules contained phosphorus, magnesium, and potassium in a ratio of 1.0:0.31:0.19. Although polyP granules are often found in cellular inclusions containing calcium[14], those isolated from *E. coli* did not contain calcium.

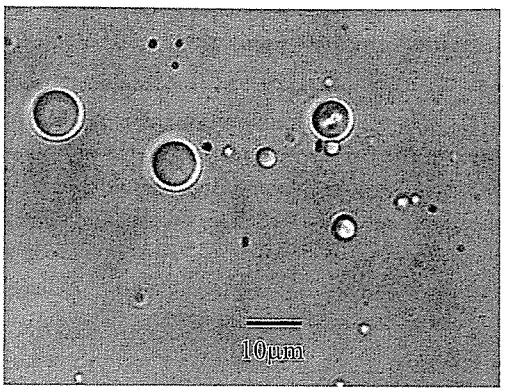

Fig. 4. Microscopic analysis of synthesized polyP granules.
The synthesized polyP granules were observed under phase-contrast microscopy.

We prepared polyP granules *in vitro* by mixing polyP, KCl, and $MgCl_2$ as to approximately the same elemental ratio as the polyP granules prepared from *E. coli* cells. The synthetic polyP granules were spherical with diameters from several hundreds of nanometers to tens of micrometers (Fig. 4). However, these synthetic polyP granules dissolved within 50 min when they were placed in HEPES buffer (data shown in Fig. 5B).

3.3. Polyamines protect polyP granules from dissolution

We suspected that polyamines protect polyP granules from dissolution in *E. coli*. We found that the polyamines such as putrescine, spermidine, and cadaverine protect the polyP granules from dissolution but that ammonium chloride does not (Fig. 5A). Igarashi and Kashiwagi predicted that 12.5 mM putrescine and 0.26 mM spermidine exist in a free form in *E. coli*[20]. The polyP granules were completely protected against dissolution by a combination of 12.5 mM putrescine and 0.26 mM spermidine (Fig. 5B).

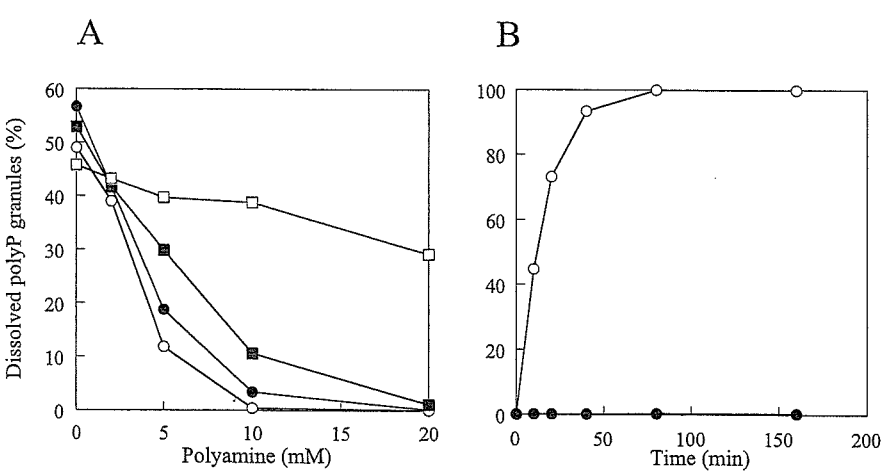

Fig. 5. Polyamines stabilize polyP granules.
(A) PolyP granules prepared *in vitro* (0.5 mg) were precipitated by centrifugation and placed in HEPES buffer containing various concentrations of putrescine (closed circular), spermidine (open circular), cadaverine (closed square), or ammonium chloride (open square). Dissolved polyP could no longer be precipitated by centrifugation. The percentage of dissolved polyP after 10-min incubation vs. total polyP granules was plotted as a function of the polyamine concentration. (B) PolyP granules prepared *in vitro* (0.5 mg) were incubated in HEPES buffer in the presence (closed) and absence (open) of 12.5 mM putrescine and 0.26 mM spermidine. The percentage of dissolved vs. total polyP granules was plotted as a function of the incubation time.

We prepared polyP granules *in vitro* by mixing polyP, KCl, and $MgCl_2$ in the presence of 10 mM spermidine. The synthetic polyP granules were very stable even when they were placed in HEPES buffer in the absence of polyamine (data not shown). These results suggested that the polyamines also interact with polyP when polyP granules are formed.

PolyP was first identified in microorganisms as metachromatic granules that are stained pink with basic blue dyes, and they were originally referred to as "volutin granule"[14]. PolyP granules from unicellular eukaryotes (*e.g.*, *Chlamydomonas reinhardtii*[25] and *Dictyostelium discoideum*[19]), a number of human pathogens (*e.g.*, malaria parasites and trypanosomatids[26]), and human platelets[27] were recently found to be surrounded by a membrane with a number of pumps and exchangers and were named acidocalcisomes. Although polyP granules are often found in cellular inclusions containing calcium[14], those isolated from *E. coli* did not contain calcium. We found that these polyP granules soon disappeared when added to buffer, although they are stabilized by polyamines (putrescine, spermidine, and spermine), which are known to be present at millimolar concentrations in both prokaryotic and eukaryotic cells[3,10]. We concluded that polyamines may interact with polyP *in vivo* and therefore affect polyP accumulation.

Our findings also suggested that, conversely, polyP accumulation may affect the intracellular levels of free polyamine. A decrease or increase in polyamine content greatly diminishes cell growth in *E. coli*[8,24], and their intracellular levels are closely regulated by control of synthesis, degradation, uptake, and excretion[9,22]. In *E. coli*, approximately 50% of putrescine and 90% of spermidine exist as polyamine-RNA complexes, and they act at the level of translation to enhance the synthesis of OppA, Cya, RpoS, FecI, and Fis[11]. Further investigations are needed to clarify the role of polyP in polyamine metabolism.

Acknowledgments

This work was supported in part by the Research and Development Program for New Bio-industry Initiatives of Bio-oriented Technology Research Advancement Institution Japan.

References

1) Ault-Riche, D., C.D. Fraley, C.M. Tzeng, and A. Kornberg. 1998. Novel assay reveals multiple pathways regulating stress-induced accumulations of inorganic polyphosphate in *Escherichia coli*. J. Bacteriol. 180: 1841–1847.
2) Clesceri, L.S., A.E. Greenberg, and R.R. Trussell. 1989. Standard methods for the examination of water and wastewater, 17th ed. American Public Health Association, Washington DC.
3) Cohen, S.S. 1998. A guide to the polyamines. Oxford University Press, Oxford, UK.
4) Datsenko, K.A., and B.L. Wanner. 2000. One-step inactivation of chromosomal genes in *Escherichia coli* K-12 using PCR products. Proc. Natl. Acad. Sci. U. S. A. 97: 6640–6645.
5) Fukuchi, J., K. Kashiwagi, M. Yamagishi, A. Ishihama, and K. Igarashi. 1995. Decrease in cell viability due to the accumulation of spermidine in spermidine acetyltransferase-deficient mutant of *Escherichia coli*. J. Biol. Chem. 270: 18831–18835.
6) Hammond, A.L. 1971. Phosphate replacements: problems with the washday miracle. Science. 172: 361–363.
7) Harold, F.M. 1960. Accumulation of inorganic polyphosphate in mutants of *Neurospora crassa*. Biochim. Biophys. Acta. 45: 172–188.
8) Igarashi, K., K. Kashiwagi, K. Kishida, T. Kakegawa, and S. Hirose. 1981. Decrease in the S1 protein of 30-S ribosomal subunits in polyamine-requiring mutants of *Escherichia coli* grown in the absence of polyamines. Eur. J. Biochem. 114: 127–131.
9) Igarashi, K., and K. Kashiwagi. 1999. Polyamine transport in bacteria and yeast. Biochem. J. 344. Pt. 3: 633–642.
10) Igarashi, K., and K. Kashiwagi. 2000. Polyamines: mysterious modulators of cellular functions. Biochem. Biophys. Res. Commun. 271: 559–564.
11) Igarashi, K., and K. Kashiwagi. 2006. Polyamine Modulon in *Escherichia coli*: Genes Involved in the Stimulation of Cell Growth by Polyamines. J. Biochem. (Tokyo) 139: 11–16.
12) Jacobson, L., M. Halmann, and J. Yariv. 1982. The molecular composition of the volutin granule of yeast. Biochem. J. 201: 473–479.
13) Jung, I.L., T.J. Oh, and I.G. Kim. 2003. Abnormal growth of polyamine-deficient *Escherichia coli* mutant is partially caused by oxidative stress-induced damage. Arch. Biochem. Biophys. 418: 125–132.
14) Kornberg, A. 1995. Inorganic polyphosphate: toward making a forgotten polymer unforgettable. J. Bacteriol. 177: 491–496.
15) Kulaev, I.S., V. Vagapov, and T. Kulakovskaya. 2004. The Biochemistry of Inorganic Polyphosphates. Wiley and Sons, NJ.
16) Kuroda, A., H. Murphy, M. Cashel, and A. Kornberg. 1997. Guanosine tetra- and pentaphosphate promote accumulation of inorganic polyphosphate in *Escherichia coli*. J. Biol. Chem. 272: 21240–21243.
17) Kuroda, A., S. Tanaka, T. Ikeda, J. Kato, N. Takiguchi, and H. Ohtake. 1999. Inorganic polyphosphate kinase is required to stimulate protein degradation and for adaptation to amino acid starvation in *Escherichia coli*. Proc. Natl. Acad. Sci. U. S. A. 96: 14264–14269.
18) Kuroda, A., K. Nomura, R. Ohtomo, J. Kato, T. Ikeda, N. Takiguchi, H. Ohtake, and A. Kornberg. 2001. Role of inorganic polyphosphate in promoting ribosomal protein degradation by the Lon protease in *E. coli*. Science. 293: 705–708.
19) Marchesini, N., F.A. Ruiz, M. Vieira, and R. Docampo. 2002. Acidocalcisomes are functionally linked to the contractile vacuole of *Dictyostelium discoideum*. J. Biol. Chem. 277: 8146–8153.
20) Miyamoto, S., K. Kashiwagi, K. Ito, S. Watanabe, and K. Igarashi. 1993. Estimation of polyamine distribution and polyamine stimulation of protein synthesis in *Escherichia coli*. Arch. Biochem. Biophys. 300: 63–68.
21) Morohoshi, T., T. Maruo, Y. Shirai, J. Kato, T. Ikeda, N. Takiguchi, H. Ohtake, and A. Kuroda. 2002. Accumulation of inorganic polyphosphate in *phoU* mutants of *Escherichia coli* and *Synechocystis* sp. strain PCC6803. Appl. Environ. Microbiol. 68: 4107–4110.
22) Pegg, A.E. 1988. Polyamine metabolism and its importance in neoplastic growth and a target for chemotherapy. Cancer. Res. 48: 759–774.
23) Pick, U., M. Bental, E. Chitlaru, and M. Weiss. 1990. Polyphosphate-hydrolysis--a protective mechanism against alkaline stress? FEBS. Lett. 274: 15–18.
24) Raj, V.S., H. Tomitori, M. Yoshida, A. Apirakaramwong, K. Kashiwagi, K. Takio, A. Ishihama, and K. Igarashi. 2001. Properties of a revertant of *Escherichia coli* viable in the

presence of spermidine accumulation: increase in L-glycerol 3-phosphate. J. Bacteriol. 183: 4493–4498.
25) Ruiz, F.A., N. Marchesini, M. Seufferheld, Govindjee, and R. Docampo. 2001. The polyphosphate bodies of *Chlamydomonas reinhardtii* possess a proton-pumping pyrophosphatase and are similar to acidocalcisomes. J. Biol. Chem. 276: 46196–46203.
26) Ruiz, F.A., C.O. Rodrigues, and R. Docampo. 2001. Rapid changes in polyphosphate content within acidocalcisomes in response to cell growth, differentiation, and environmental stress in *Trypanosoma cruzi*. J. Biol. Chem. 276: 26114–26121.
27) Ruiz, F.A., C.R. Lea, E. Oldfield, and R. Docampo. 2004. Human platelet dense granules contain polyphosphate and are similar to acidocalcisomes of bacteria and unicellular eukaryotes. J. Biol. Chem. 279: 44250–44257.
28) Sedlak, R.I. 1991. Phosphorus and nitrogen removal from municipal wastewater, 2nd ed. Lewis publishers, Florida.
29) Tabor, H., E.W. Hafner, and C.W. Tabor. 1980. Construction of an *Escherichia coli* strain unable to synthesize putrescine, spermidine, or cadaverine: characterization of two genes controlling lysine decarboxylase. J. Bacteriol. 144: 952–956.

Cellular and Molecular Biology™ 52, N°4,23-29
DOI 10.1170/T724

ISSN 1165-158X
2006 Cell. Mol. Biol.™

INORGANIC POLYPHOSPHATE STIMULATES LON-MEDIATED PROTEOLYSIS OF NUCLEOID PROTEINS IN *ESCHERICHIA COLI*

K NOMURA[1], J KATO[1], N TAKIGUCHI[1], H OHTAKE[2], and A KURODA[1,3]*

[1]*Department of Molecular Biotechnology, Hiroshima University, Hiroshima 739-8530, Japan
Fax: (+81)82-424-7047; E-mail: akuroda@hiroshima-u.ac.jp
[2]Department of Biotechnology, Osaka University, Osaka 565-0871, Japan
[3]PRESTO, Japan Science and Technology Corporation, Kawaguchi, Saitama 332-0012, Japan

Received ??th, 2005; Accepted ??th, 2005; Published May 30th, 2006

Abstract – Inorganic polyphosphate (polyP) accumulates in response to amino acid starvation in *Escherichia coli*.Previously, we found that the complex formation of Lon with polyP stimulates proteolysis of free ribosomalproteins. In the current studies, we examined the effects of polyP on the degradation of major nucleoid proteins.Fusions of green fluorescent protein with HimA, Fis, HupA, and HupB were clearly associated with polyP *invivo*. Lon degraded His-tagged HimA protein only in the presence of polyP *in vitro* as well as *in vivo*.Whereas, when HimA and HimD formed a heterodimer, Lon could not degrade it even in the presence of polyP.In addition, Lon degraded His-tagged Fis protein in the presence of polyP. However, *in vivo*, Lon did notefficiently degrade the Fis protein even when cells accumulated polyP in response to amino acid starvation. Itappears that this is due to tighter binding of Fis to DNA than to polyP and resistance of the DNA-Fis toLon-mediated proteolysis. Indeed, we found that at least a five-fold excess of polyP was necessary to displaceDNA from the DNA-Fis complex. Furthermore, Lon degraded His-tagged HupA protein efficiently in thepresence of polyP. We also showed that degradation of the translational initiation factor InfC depends onpolyP.

Key words: Polyphosphate, Lon, Nucleoid protein.

INTRODUCTION

In prokaryotes such as *Escherichia coli*, amino acid starvation causes coupled cessation of protein and stable RNA synthesis, a process called the"stringent response" (5). In addition, the rate of protein degradation increases under conditions of amino acid starvation (26,36). If the environment is suddenly depleted of amino acids, new enzymes can be synthesized only from amino acids liberated by protein turnover (38). These metabolic responses are very important for allowing cells to escape from amino acid starvation and to adapt to new environmental conditions.

Previously, we found that polyphosphate (polyP), which is a linear polymer of many hundreds of orthophosphate residues, accumulates during the stringent response in *E. coli* (23). An *E. coli* mutant deficient in polyP kinase (PPK), the principal enzyme for the synthesis of polyP, fails to increase protein turnover and shows an extended lag in growth when shifted from a nutrient-rich to a nutrient-poor medium(nutritional downshift) (25). These studies suggested that protein degradation is triggered by the accumulation of polyP in *E. coli*. Starvation-induced proteolysis is an energy- dependent process requiring the hydrolysis of ATP (27). The ATP-dependent protease Lon, conserved from bacteria to humans, is responsible for the rapid turnover of both abnormal and naturally unstable proteins (16,25). We found that mutations in both the Lon and Clp proteases produce the same phenotype as *ppk* mutations and that addition of amino acids overcomes the block in these cases (24). PolyP forms a complex with Lon, which enables Lon to degrade free ribosomal proteins (24). Certain very abundant ribosomal proteins could be the principal sacrificial substrates targeted for degradation at the onset of the downshift. However, the increase in total protein turnover during starvation could not be ascribed only due to the degradation of free ribosomal proteins.

Previously, we found that the interaction of ribosomal proteins with polyP seems necessary for the stimulation of Lon-mediated proteolysis (24,30). PolyP in the polyP-Lon complex may function as an adaptor molecule to capture substrates that are able to bind to polyP. PolyP is a phosphate polymer with some similarity to RNA and DNA, and, therefore, it seems reasonable that polyP readily interacts with basic proteins such as histones (21). Currently, four structural proteins, IHF (integration host factor), Fis (factor for inversion stimulation), H-NS (histone-like nucleoid structuring protein), and HU (heat-stable nucleoid protein composed of HupA and HupB) as well as one stationary-phase-specific DNA-binding protein, Dps (DNA binding protein

Abbreviations: **DAPI**: 4',6-diamidino-2-phenylindole; **polyp**: inorganicpolyphosphate; **IPTG**: isopropyl-β-D-thiogalactopyranoside; **GFP**: green fluorescence protein; **IHF**: HimA and HimD heterodimer; **HU**: HupA andHupB heterodimer; **MOPS**: 3-(N-Morpholino) propanesulfonic acid; **PPK**: polyphosphate kinase.

from starved cells), are thought to be the major components of the *E. coli* nucleoid (8,33). Here, we examined whether these nucleoid proteins are associated with polyP *in vivo* and whether they are degraded by the polyP-Lon complex. We also tested seven additional nucleoid-associated proteins (2), including CbpA (curved DNA-binding protein A), CbpB (curved DNA-binding protein B), DnaA (DNA replication protein A or initiator protein), Hfq (host factor for phage Q), IciA (inhibitor of chromosome initiation A), Lrp (leucine-responsive regulatory protein), and StpA (suppresser of Td phenotype) for association with polyP and degradation by the polyP-Lon complex.

MATERIALS AND METHODS

Monitoring of Subcellular Localization of Nucleoid Protein-Green Fluorescent Protein (GFP) Fusions.

A complete set of *E. coli* K-12 open reading frame archive (ASKA) library with GFP and His tags was constructed at the Nara Institute of Science and Technology, Japan (20). From this library, plasmids encoding HimA, HimD, Fis, Hns, HupA, HupB, Dps, CbpA, CbpB, DnaA, Hfq, IciA, Lrp, and StpA proteins fused with GFP were selected and then transferred into *E. coli* MT4 (*phoU*) (28). The transformants were grown on a 3-(N-morpholino) propanesulfonic acid (MOPS) minimal medium (25) containing 0.1mM isopropyl-β-D-thiogalactopyranoside (IPTG) and 20mg/l chloramphenicol for 4hrs at 37°C. Cells were stained with 4',6-diamidino-2-phenylindole (DAPI) at a concentration of 5mg/l and kept on ice for 30min. Cells were fixed with 1% agarose and then observed under fluorescent microscopy. Fluorescence micrographs were recorded on an Olympus BX60 microscope equipped with a 100X UPlanApo objective. Two filter sets were used: a MNIBA filter for GFP (470-490nm) and a MWU filter for DAPI (330-385nm). Images were captured using a cooled charge-coupled device camera DP70 (Olympus Co., Tokyo, Japan). Images were processed using Adobe Photoshop 6.0.

Protein Purification

DNA fragments of *himA*, *himD*, *hupA*, and *hupB* which were amplified by PCR using himA1 and himA2, himD1 and himD2 hupA1 and hupA2, and hupB1 and hupB2 primers, respectively (Table 1), were inserted into the *Nco*I and *Xho*I sites of pET21-b (Novagen, San Diego, CA).

Table 1 DNA sequence of primers

Primer	DNA sequence
himA1	TAACCATGGCGCTTACAAAAGCTGA
himA2	CCGCTCGAGCTCGTCTTTGGGCGAAGCGT
himA3	TGTTCTAGAAACTCGTCTTTGGGCGAAGCGT
himA4	CCGAGATCTGCTAACAGGAGGAATTAAC
himA5	ACGGAATTCTCACAGATCCTCTTCTGAGATGA
himD1	ACTGGTCTCACATGACCAAGTCAGAATTGA
himD2	CCGCTCGAGACCGTAAATATTGGCGCGATC
himD3	TGTTCTAGAAAACCGTAAATATTGGCGCGATC
himD4	CCGAGATCTTCAGTGGTGGTGGTGGTGGT
hupA1	TAACCATGGGGAACAAGACTCAACTGATTGA
hupA2	CCGCTCGAGCTTAACTGCGTCTTTCAGTG
hupA3	TGTTCTAGAAACTTAACTGCGTCTTTCAGTG
hupB1	TAACCATGGTGAATAAATCTCAATTGATC
hupB2	CCGCTCGAGGTTTACCGCGTCTTTCAGTG

These plasmids were designated pET-HimA, pET-HimD, pET-HupA, and pET-HupB, respectively. HimA, HimD HupA, and HupB proteins with C-terminal His tags were expressed in *E. coli* recombinants that harbored pET-HimA, pET-HimD, pET-HupA, and pET-HupB, respectively. To express the HimA and HimD heterodimer (IHF), both the *himA* fragment amplified with himA4 and himA5 primers and the *himD* fragment amplified with himD1 and himD4 primers were inserted into *Nco*I and *Eco*RI sites of pBAD/Myc-HisB (Invitrogen, Carlsbad, CA). This plasmid was designated pBAD-IHF. His tagged proteins were purified using chromatography on a HiTrap Chelating column (Amersham Biosciences, Piscataway, NJ). The fractions containing nucleoid proteins were dialyzed against a 50mM HEPES-NaOH (pH 7.4) buffer containing 1mM EDTA (pH 7.4) and 20% glycerol solution, and then applied to HS/M cation exchange column (POROS, Perspective Biosystems, Cambridge, MA). The nucleoid proteins were eluted from the column with a linear gradient of 0 to 1M NaCl in the buffer.

Protein Degradation

Purified proteins (5μg) and Lon (1μg) were incubated in a 10μl buffer containing 25mM Tris-HCl (pH 7.8), 5mM MgCl2, and 4mM ATP in the presence and absence of polyP700 (1μg, 14pmol as a polymer) at 37°C and then separated by 12.5% sodium dodecyl sulfate-polyacrylamide gel electrophoresis. PolyP700 was synthesized by PPK with ATP as a substrate as described previously (23). After electrophoresis, proteins were stained with SYPRO Orange (Molecular Probes, Eugene, OR) and visualized with a Typhoon image analyzer (Amersham Biosciences).

Monitoring in vivo Degradation

DNA fragments of *himA* and *himD*, which were amplified by PCR with himA1 and himA3 primers and himD1 and himD3 primers, respectively (table 1), were inserted into the *Nco*I and *Xba*I sites of pBAD/Myc-HisB (Invitrogen, Carlsbad, CA). These plasmids were designated pBAD-HimA and pBAD-HimD, respectively. HimA and HimD with C-terminal myc epitope fusion were expressed in the wild-type, *ppk*, *lon*, and *clp* mutants of *E. coli* harbouring pBAD-HimA and pBAD-HimD on 2xYT medium (34) for 2hrs in the presence of 0.2% L-arabinose. To express HimA and HimD simultaneously, pBAD-IHF was introduced into the wild-type and *ppk* mutant cells. To express HupA, a *hupA* DNA amplified by PCR with himA1 and himA3 primers was inserted into the *Nco*I and *Xba*I sites of pBAD/Myc-HisB. This plasmid was designated as pBAD-HupA. Plasmids pHis-Fis and pHis-InfC were constructed from pHis-fis-GFP and pHis-InfC-GFP (ASKA library) by removing the *Not*I fragment that encodes GFP. Fis and InfC proteins with an N-terminal His tag were expressed on 2xYT medium for 2hrs in the presence of 20μM IPTG. Cells were collected by centrifugation and resuspended in the MOPS minimal medium. At the indicated times, total protein (100μl of the culture) was subjected to sodium dodecyl sulfate-polyacrylamide gel electrophoresis and transferred onto a polyvinylidene fluoride membrane. Western analysis was performed with an antibody to His tag or myc epitope (Santa Cruz Biotechnology, Inc., Santa Cruz, CA, USA) and ECL Western blotting detection reagents (Amersham Bioscience). Immunoreactive proteins were detected with X-ray film. Gel Shift Assay. A synthetic double-stranded rrnB-P1-DNA (AGGCTGATTTGGTTGAATGTTGCGCGGTCAGAAAA) was used for the gel shift assay. Fis protein, rrnB-P1-DNA, and polyP were mixed in a 10μl solution of 25mM Tris-HCl (pH 7.8) and 5mM MgCl2 for 5min at room temperature and then separated byelectrophoresis on a polyacrylamide gel. Electrophoresis was performed with a buffer of 25mM Tris and 192mM glycine, and then stained with ethidium bromide to detect DNA.

RESULT

In vivo PolyP-Binding Assay for Nucleoid Proteins.

The level of polyP accumulated in *E. coli* MG1655 (wild-type) growing on a rich medium is approximately 1nmol/mg protein. When shifted to a

nutrient-poor medium (e.g., MOPS medium), the wild-type accumulates approximately 50-100nmol polyP/mg protein. Following 4hrs of this nutritional downshift, the level decreases 2-3nmol polyP/mg protein (25). While, *E. coli* MT4 (*phoU*) mutant accumulates approximately 200-500nmol polyP/mg protein constitutively (28) and forms polyP particles that can be observed easily by fluorescent microscopy (green-yellow fluorescence in fig. 1).

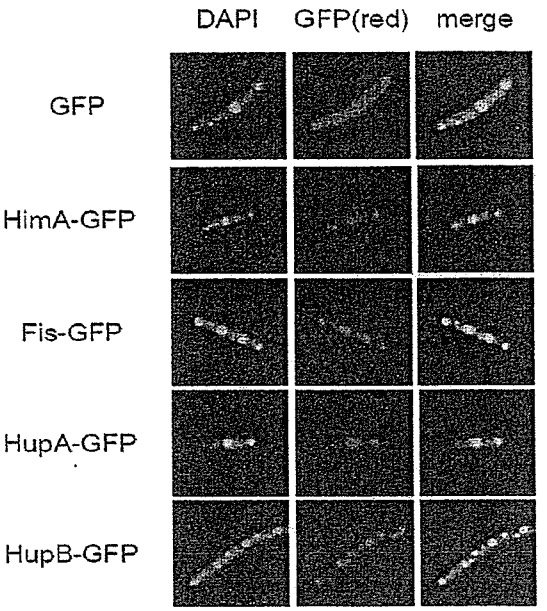

Fig. 1. *In vivo* polyP-binding assay using a polyP-accumulating strain and a GFP-fusion protein. *E. coli* MT4 (*phoU*) carrying a GFP fusion gene was grown on a MOPS minimal medium. DAPI fluorescence was used to detect nucleoids (blue) and polyP (green-yellow) under UV light (330-385nm). GFP shows green fluorescence under blue light (470-490nm) but was changed to red using Adobe Photoshop.

These cells were also costained with DAPI to detect nucleoids (blue fluorescence). GFP, in contrast, was found throughout the cell because it does not bind to polyP. Therefore, GFP fusion proteins can be used to assess polyP binding *in vivo*. Specifically, if a test protein is associated with polyP *in vivo*, its GFP fusion would be localized in the polyP particles. Therefore, we grew *E. coli* MT4 carrying GFP fusion genes on the MOPS minimal medium and observed them under fluorescent microscopy. We found that HimA, Fis, HupA, and HupB fusion proteins linked at their C-termini to GFP were localized in the polyp granules (fig. 1). In contrast, HimD, Hns, Dps, CbpA, CbpB, DnaA, Hfq, IciA, Lrp, and StpA were not localized in the polyP particle.

Degradation of HimA Protein by Lon

Because our initial results suggested that HimA protein, but not HimD protein, is a polyP-binding protein *in vivo*, we examined their ability to be cleaved by Lon-dependent proteolysis in the absence and presence of polyP. Lon degraded purified HimA with C-terminal His tag (HimA-His) only in the presence of polyP (fig. 2). Lon degraded purified HimD with C-terminal His tag (HimD-His), although the cleavage was not dependent on polyP (fig. 2).

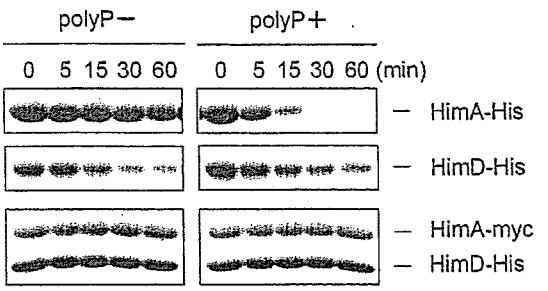

Fig. 2 *In vitro* degradation of HimA protein by Lon in the absence and presence of polyP. HimA-His, HimD-His, or IHF (HimA-myc and HimD-His dimer) (5μg) were mixed with Lon (1μg) in a 10μl solution containing 25mM Tris-HCl (pH 7.8), 5mM MgCl2, and 4mM ATP. PolyP (1μg) was used to stimulate Lon-mediated protein degradation.

In vivo, HimA exists not only as a homodimer but also as a heterodimer with HimD, which is called IHF. We simultaneously expressed HimA with a C-terminal myc epitope (HimA-myc) and HimD-His, and then purified the IHF heterodimer using a HiTrap Chelating column. We used the HimA-myc to omit contamination of the HimA dimer under these conditions. Interestingly, Lon did not degrade IHF heterodimer (fig. 2). Thus, HimA was degraded in the presence of polyP but not when it formed a heterodimer with HimD. To monitor *in vivo* degradation, we expressed HimA protein with a C-terminal myc epitope (HimA-myc-His) in the wild-type, *ppk*, *lon*, and *clp* mutant cells. These cells were then subjected to amino acid starvation. Degradation of HimA-myc-His protein was monitored by Western blotting. As expected, degradation of HimA-myc-His protein was dependent on both PPK and Lon *in vivo* (fig. 3).

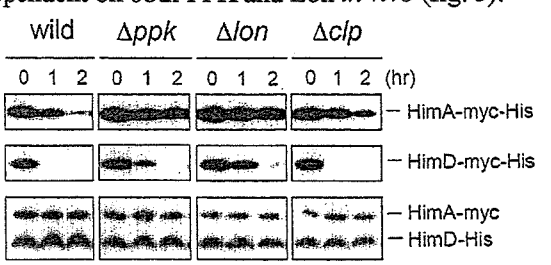

Fig. 3 *In vivo* degradation of HimA and HimD proteins in response to nutritional downshift. HimA-myc-His, HimD-myc-His, and IHF (HimA-myc, HimD-His) proteins were expressed in the wild-type, *ppk*, *lon*, and *clp* mutant strains on a rich medium and then shifted to a MOPS minimal medium (nutritional downshift). Western blot analysis was performed using an antibody against His-tag or myc epitope.

HimD protein with C-terminal myc epitope (HimD-myc-His) was degraded much more quickly *in vivo* than HimA-myc-His. When the IHF heterodimer was formed, it was very stable even in the wild-type (fig. 3).

Degradation of Fis Protein by Lon

Lon also degraded purified Fis proteins with N-terminal His tags (His-Fis) only in the presence of polyP (Fig. 4).

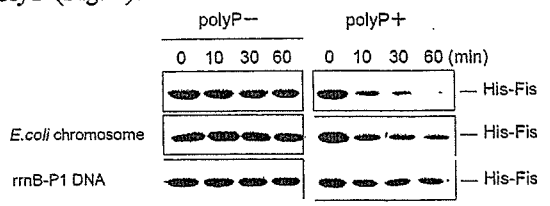

Fig. 4 *In vitro* degradation of Fis protein by Lon in the absence and presence of polyP. His-Fis protein (4μg; 235pmol) was mixed with Lon (1μg; 11pmol) in a 10μl solution containing 25mM Tris-HCl (pH 7.8), 5mM MgCl2, and 4mM ATP. PolyP (1μg; 14pmol) was used to stimulate Lon-mediated protein degradation. *E. coli* chromosomal DNA (1.2μg) and *rrnB*-P1 DNA (1.2μg; 52pmol) was used to inhibit proteolysis.

To monitor *in vivo* degradation of Fis, we expressed the His-tagged Fis protein in wild-type and *ppk* mutant cells. Unexpectedly, it was stable even in the wild-type cells (fig. 5).

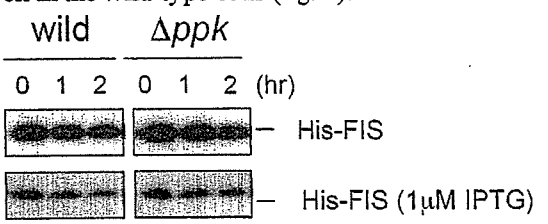

Fig. 5 *In vivo* degradation of Fis protein. His-Fis protein was expressed in the wild-type and *ppk* mutant strains on a rich medium and then subjected to the downshift. Western blot analysis was performed using an antibody against His tag.

In addition, when it was induced by a low concentration of IPTG (1μM), *ppk* had very little effect on its degradation *in vivo* (Fig. 5). *E. coli* chromosomal DNA partially rescued polyP-Lon-mediated proteolysis of His-Fis (Fig. 4). It is known that Fis protein specifically binds to *rrnB*-P1 DNA (19). The *rrnB*-P1 DNA more strongly rescued polyP-Lon-mediated proteolysis (Fig. 4). We examined the formation of a DNA-Fis complex using a gel shift assay. In the presence of a five-fold excess of His-Fis to DNA, almost all of the *rrnB*-P1 DNA was shifted (Fig. 6A). Because polyp binds to Fis, it is able to compete with DNA for the binding to Fis. However, at least a five-fold molar excess of polyP to DNA is necessary to inhibit the formation of the *rrnB*-P1 DNA-Fis complex (Fig. 6B). Therefore, when 14pmol of polyP was mixed with 52pmol *rrnB*-P1 DNA (the condition in fig. 4), the majority of Fis was complexed with DNA. These results indicated that the polyP-Fis is degraded by Lon, but the DNA-Fis complex is resistant to Lon-mediated proteolysis.

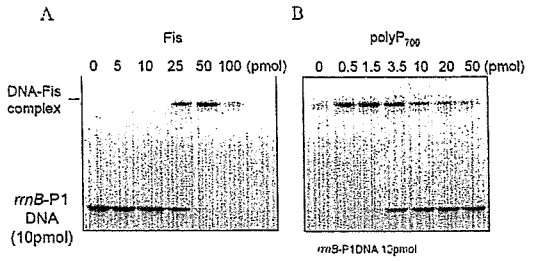

Fig. 6 DNA-Fis complex in the presence of polyP. *A*, A synthesized *rrnB*-P1 DNA (10pmol) and various amount of His-Fis protein were mixed and then subjected to polyacrylamide gel electrophoresis. *B*, The synthesized *rrnB*-P1 DNA (10pmol), Fis protein (100pmol), and various amount of polyP were mixed and then subjected to polyacrylamide gel electrophoresis. DNA was stained with ethidium bromide.

Degradation of HupA and HupB Proteins by Lon

Lon degraded purified HupA with a C-terminal His tag (HupA-His) and polyP stimulated its cleavage (fig. 7). Lon degraded purified HupB with a C-terminal His tag (HupB-His), although the cleavage was not dependent on polyP (fig. 7).

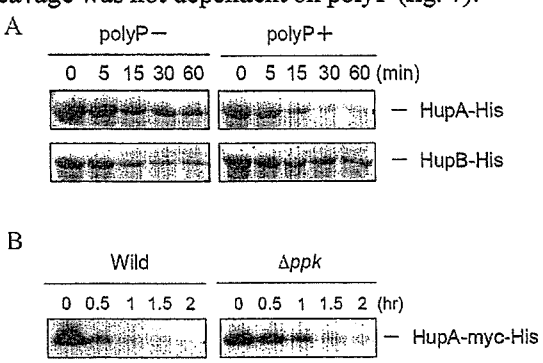

Fig. 7 Degradation of HupA and HupB proteins. *A*, HupA-His and HupD-His (5μg) were mixed with Lon (1μg) in a 10μl solution containing 25mM Tris-HCl (pH 7.8), 5mM MgCl2, and 4mM ATP. PolyP (1μg) was used to stimulate Lon-mediated protein degradation. *B*, HupA-myc-His protein was expressed in the wild-type and *ppk* mutant strains on a rich medium and then subjected to the downshift. Western blot analysis was performed using an antibody against myc epitope.

In vivo, degradation of HupA protein with a C-terminal myc epitope (HupA-myc-His) in the wild-type was faster than in the *ppk* mutant cells during amino acid starvation (fig. 7).

PolyP-dependent Degradation of InfC

In vitro experiments in Kornberg's (A. Kornberg and R. Ohtomo, personal communication) and our

laboratories have identified not only histone-like proteins as polyP-binding proteins, but also InfC and InfB (translational initiation factors); Lon and ClpB (chaperon and protease); RpoD, SrmB, Rnr, RluC and Gyr (RNA- and DNA-related enzymes); YabC and YbiB (unknown function); LpdA (pyruvate dehydrogenase complex); and SucA (2-oxoglutarate dehydrogenase). We therefore analyzed whether these proteins are associated with polyP and whether their degradation *in vivo* is dependent on polyP. Our *in vivo* assay showed that C-terminal GFP fusions of LpdA, RluC, and InfC associated with polyP. In addition, InfC protein with an N-terminal His tag was degraded in the wild-type after the nutritional downshift, whereas it was very stable in the *ppk* mutant (fig. 8). These results indicated that polyP-Lon degrades InfC.

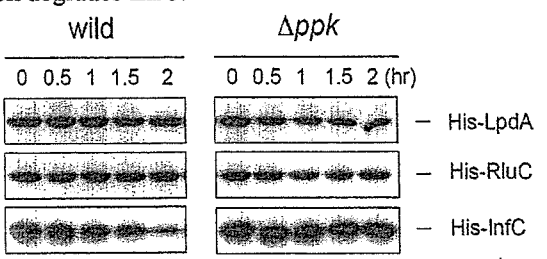

Fig. 8 *In vivo* degradation of InfC protein. His-LpdA, His-RluC, and His-InfC were expressed on a rich medium and then subjected to the downshift. The Western analysis was performed using an antibody against His tag.

DISCUSSION

Cells balance energy-efficient growth with the ability to adapt rapidly to sudden changes in their environment. In an environment rich in amino acids, cells do not expend energy for making amino acid biosynthetic enzymes. If the environment becomes depleted of amino acids, cells use their own proteins as sources of amino acids to generate amino acid biosynthetic enzymes and to adapt to amino acid starvation. In the recent studies (23,24,25,30), we provide several lines of evidence that polyP and Lon protease are involved in this starvation-induced proteolysis in *E. coli*: i) the *ppk* and *lon clp* mutants fail to activate starvation-induced proteolysis; ii) polyP, which accumulates in response to amino acid starvation, forms a complex with Lon; and iii) formation of the complex enables Lon to degrade free ribosomal proteins. Certain very abundant ribosomal proteins could be the sacrificial substrates targeted for degradation at the onset of the downshift. However, we could not ascribe the increase in total protein turnover during starvation exclusively to degradation of free ribosomal proteins. Indeed, in the current studies, we found that polyP-Lon complex degrades major nucleoid proteins, such as HimA, Fis, and HupA, and the translational initiation factor, InfC. The degradation of these proteins may contribute to the amino acid supply when the cells are starved for amino acids. HimA is a subunit of IHF, which was originally discovered as an essential protein for the integration of phage lambda DNA into the chromosome (29). Another subunit of IHF is HimD, which show 30% amino acid sequence identity with HimA. IHF is now known to be involved in a variety of other processes, such as activation of transcription in phages (15,17) and *E. coli* (10), transposition (31,35), DNA replication (13,19), partitioning (12), and lambda packaging (22). Although IHF is mainly a heterodimeric protein, HimA and HimD can also exist as homodimers, which specifically recognize the same *ihf* sequence (39). However, neither HimA nor HimD homodimers can substitute for the function of the heterodimer *in vivo* (11). Therefore, it is unclear whether the Lon-mediated proteolysis of the HimA homodimer directly affects the function of IHF. IHF also shares significant homology with the subunits of another heterodimeric histone-like protein, HU, which is composed of HupA and HupB (8). HU is also involved in many cellular processes, such as DNA replication, recombination, and transcription as likely as IHF (8). In contrast to IHF, the HupA and HupB homodimers are functionally active and the composition of HU varies throughout the growth phase. Although the HupA homodimer prevails during exponential growth phase, the HupA and HupB heterodimer becomes predominant in stationary phase (7). Furthermore, the function of the heterodimer is required for long-term survival (7). Recently, it was also reported that the composition of HU changes during cold shock (14). Therefore, Lon-mediated proteolysis of the HupA homodimer might be important in the regulation of HU. Fis is the most abundant nucleoid protein in exponentially growing *E. coli* cells (60000 molecules/cell or 1 Fis dimer for every 200 to 300bp DNA segment) (1). Fis binds to AT-rich DNA sequences, which are located upstream of genes, induces DNA-bending, and enhances the expression of genes such as rRNA and tRNA in rapidly growing cells (9,37). It is known that the intracellular levels of Fis in growing cells decreases in the stationary phase. Because the polyP-Lon complex degraded the His-Fis protein *in vitro*, we expected that the His-Fis fusion protein is rapidly degraded after the nutritional downshift. However, His-Fis was not degraded rapidly even in the wild-type after the downshift. Furthermore, we found that a DNA-Fis complex is resistant to Lon-mediated proteolysis. Although polyP competed with DNA for the binding to Fis, the intracellular level of polyP might not be high enough to remove

Fis from DNA-Fis complexes. Recently, we found that ClpAP is involved in the rapid degradation of Fis under starvation conditions (K. Nomura and A. Kuroda, unpublished results), and we are now investigating the mechanism. InfC is the translational initiation factor, IF3, that is believed to be essential for selection of the initiation codon by monitoring the pairing between the initiator fMet-tRNA and the initiation codon (18). If this pairing is good, as in an AUG start codon, IF3 stabilizes the translation initiation complex and translation initiation proceeds. If the codon is suboptimal, IF3 destabilizes this complex and translation initiation is disfavored (3). IF3 is autoregulated through use of its unique AUU initiation codon (4). IF3 may also be targeted for Lon-mediated proteolysis as the free ribosomal proteins were degraded during amino acid starvation.

Acknowledgments – We thank Drs. H. Mori and H. Niki for providing ASKA library, and Drs A. Kornberg and R. Ohtomo for providing unpublished results on polyP-binding proteins. This work was supported in part by a Grant-in-Aid from the Ministry of Education, Science, Sports, and Culture of Japan.

REFERENCES

1. Ali Azam. T., Iwata, A., Nishimura, A., Ueda,S. and Ishihama, A., Growth phase-dependent variation in protein composition of the Escherichia coli nucleoid. *J. Bacteriol.* 1999, **181**:6361-6370.
2. Azam, T. A., Hiraga, S. and Ishihama, A., Twotypes of localization of the DNA-binding proteinswithin the *Escherichia coli* nucleoid. *Genes Cells.* 2000, **5**:613-626.
3. Berkhout, B., van der Laken, C. J. and van Knippenberg, P. H., Formylmethionyl-tRNA binding to 30 S ribosomes programmed with homopolynucleotides and the effect of translational initiation factor 3. *Biochim. Biophys. Acta.* 1986, **866**:144-153.
4. Butler, J. S., Springer, M. and Grunberg-Manago, M., AUU-to-AUG mutation in the initiator codon of the translation initiation factor IF3 abolishes translational autocontrol of its own gene (*infC) in vivo. Proc. Natl. Acad. Sci. U S A* 1987, **84**:4022-4025.
5. Cashel, M. and Kalbacher, B., The control of ribonucleic acid synthesis in *Escherichia coli.* V. Characterization of a nucleotide associated with the stringent response. *J. Biol. Chem.* 1970, **245**:2309-2318.
6. Chung, C. H. and Goldberg, A. L., DNA stimulates ATP-dependent proteolysis and protein-dependent ATPase activity of protease La from *Escherichia coli. Proc. Natl. Acad. Sci. U S A* 1982, **79**:795-799.
7. Claret, L. and Rouviere-Yaniv, J., Variation in HU composition during growth of *Escherichia coli*: the heterodimer is required for long term survival. *J. Mol. Biol.* 1997, **273**:93-104.
8. Drlica, K. and Rouviere-Yaniv, J., Histonelike proteins of bacteria. *Microbiol. Rev.* 1987, **51**:301-319.
9. Finkel, S. E. and Johnson, R. C., The Fis protein: it's not just for DNA inversion anymore. *Mol. Microbiol.* 1992, **6**:3257-3265.
10. Freundlich, M., Ramani, N., Mathew, E., Sirko, A. and Tsui, P., The role of integration host factor in gene expression in *Escherichia coli. Mol. Microbiol.* 1992, **6**:2557-2563.
11. Friedman, D. I., Integration host factor: a protein for all reasons. *Cell* 1988, **55**:545-554.
12. Funnell, B. E., Participation of *Escherichia coli* integration host factor in the P1 plasmid partition system. *Proc. Natl. Acad. Sci. U S A* 1988, **85**:6657-6661.
13. Gamas, P., Burger, A. C., Churchward, G., Caro, L., Galas, D. and Chandler, M., Replication of pSC101: effects of mutations in the *E. coli* DNA binding protein IHF. *Mol. Gen. Genet.* 1986, **204**:85-89.
14. Giangrossi, M., Giuliodori, A. M., Gualerzi, C. O. and Pon, C. L., Selective expression of the beta-subunit of nucleoid-associated protein HU during cold shock in *Escherichia coli. Mol. Microbiol.* 2002, **44**:205-216.
15. Giladi, H., Gottesman, M. and Oppenheim, A. B., Integration host factor stimulates the phage lambda pL promoter. *J. Mol. Biol.* 1990, **213**:109-121.
16. Goldberg, A. L., The mechanism and functions of ATP-dependent proteases in bacterial and animal cells. *Eur. J. Biochem.* 1992, **203**:9-23.
17. Goosen, N. and van de Putte, P., Regulation of Mu transposition. I. Localization of the presumed recognition sites for HimD and Ner functions controlling bacteriophage Mu transcription. *Gene* 1984, **30**:41-46.
18. Gualerzi, C., Risuleo, G. and Pon, C. L., Initial rate kinetic analysis of the mechanism of initiation complex formation and the role of initiation factor IF-3. *Biochemistry* 1977, **16**:1684-1689.
19. Hwang, D. S. and Kornberg, A., Opening of the replication origin of *Escherichia coli* by DnaA protein with protein HU or IHF. *J. Biol. Chem.* 1992, **267**:23083-23086.
20. Kitagawa, M., Ara, T., Arifuzzaman, M., Ioka-Nakamichi, T., Inamoto, E., Toyonaga, H. and Mori, H., Complete set of ORF clones of *Escherichia coli* ASKA library (A Complete Set of *E. coli* K-12 ORF Archive): Unique Resources for Biological Research. *DNA Research* 2005, in press.
21. Kornberg, A., Inorganic polyphosphate: toward making a forgotten polymer unforgettable. *J. Bacteriol.* 1995, **177**:491-496.
22. Kosturko, L. D., Daub, E. and Murialdo, H., The interaction of *E. coli* integration host factor and lambda cos DNA: multiple complex formation and protein-induced bending. *Nucleic Acids Res.* 1989, **17**:317-334.
23. Kuroda, A., Murphy, H., Cashel, M. and Kornberg, A., Guanosine tetra- and pentaphosphate promote accumulation of inorganic polyphosphate in *Escherichia coli. J. Biol. Chem.* 1997, **272**:21240-21243.
24. Kuroda, A., Nomura, K., Ohtomo, R., Kato, J., Ikeda, T., Takiguchi, N., Ohtake, H. and Kornberg,